Jinst

Published by IOP Publishing for Sissa Medialab

Received: *March 31, 2023*
Accepted: *May 24, 2023*
Published: *June 29, 2023*

Snowmass'2021 Accelerator Frontier

Superconducting detector magnets for high energy physics

M. Mentink,[a,*] K. Sasaki,[b] B. Cure,[a] N. Deelen,[a] A. Dudarev,[a] M. Abe,[b] M. Iio,[b] Y. Makida,[b] T. Okamura,[b] T. Ogitsu,[b] N. Sumi,[b] A. Yamamoto,[b] M. Yoshida[b] and H. Iinuma[c]

[a] *CERN,*
1211 Geneva 23, Switzerland
[b] *KEK,*
1-1 Oho, Tsukuba, Japan
[c] *Graduate School of Science and Engineering, Ibaraki University,*
162-1 Shirakata, Toka-mura, Japan

E-mail: matthias.mentink@cern.ch

Abstract: Various superconducting detector solenoids for particle physics have been developed in the world. The key technology is the aluminum-stabilized superconductor for almost all the detector magnets in particle physics experiments. The coil fabrication technology is also important and it has advanced along with the conductor technology, such as the inner coil winding technique, indirect cooling, transparent vacuum vessel, quench protection scheme using pure aluminum strips and so on. The detector solenoids design study is in progress for future big projects in Japan and Europe, that is, ILC (International Linear Collider), FCC (Future Circular Collider) and CLIC (Compact LInear Collider), based on the technologies established over many years. The combination of good mechanical properties and keeping a high RRR is a key point for the development of Al-stabilized conductor. The present concern for the detector solenoid development is to have been nearly losing the key technologies and experiences. Nowadays, there are no industrial companies having the capacity to manufacture such aluminum stabilized superconductor. Complementary efforts are seriously required to re-realize and validate the performance required in the future projects in collaboration with worldwide institutes and industries. Some mid-scale physics experiments required detector solenoids wound with not aluminum stabilized conductor but conventional copper stabilized conductor. The specific requirement is to control the magnetic field distribution precisely, and the efforts to realize the requirement are on going with regard to the magnetic field design technology with high precision simulation, coil fabrication technology and so on.

*Corresponding author.

https://doi.org/10.1088/1748-0221/18/06/T06013

2023 JINST 18 T06013

KEYWORDS: Acceleration cavities and superconducting magnets (high-temperature superconductor, radiation hardened magnets, normal-conducting, permanent magnet devices, wigglers and undulators); Instrumentation for particle accelerators and storage rings - high energy (linear accelerators, synchrotrons); Instrumentation for particle accelerators and storage rings - low energy (linear accelerators, cyclotrons, electrostatic accelerators)

ARXIV EPRINT: 2203.07799

2023 JINST 18 T06013

Contents

1 Introduction **1**

2 Technology for detector magnets **2**
- 2.1 Aluminum stabilized superconductor and superconducting coil 3
- 2.2 Inner winding technique to support cylinder and indirect/conduction cooling 4
- 2.3 Energy/Mass ratio and transparency 5
- 2.4 Thermal stabilization and fast quench propagation by using pure-Al strips 8
- 2.5 Transparent vacuum vessel 9

3 Future prospects for detector solenoid technology **11**

4 Future projects **13**
- 4.1 Detectors for high energy physics 13
  - 4.1.1 FCC-ee 13
  - 4.1.2 FCC-hh 17
  - 4.1.3 CLIC 20
  - 4.1.4 ILD 23
  - 4.1.5 SID 25
- 4.2 Detectors for secondary particle experiments 26
  - 4.2.1 COMET 26
  - 4.2.2 J-PARC g-2/EDM 28

5 Summary **31**

1 Introduction

A superconducting detector magnet is one of the key components for particle physics experiments to analyze the momentum and polarity of charged particles. It is required to have a large warm bore to install many types of particle detectors, and a large solid angle to maximize the detection efficiency of particles. Many magnets have been developed since 1977 [1]. Table 1 summarizes the advances in thin detector solenoids. Figure 1 shows general parameters and configuration of the ATLAS-CS and CMS detector solenoids at the CERN LHC experiments representing most recent advances [1].

Design studies of superconducting detector solenoids are progressing for the several future projects. The target central field is generally 2–5 T, which is mainly determined by the resolution of particle detector systems. Superconducting detector magnets can be roughly categorized into two types, considering the required feature based on the arrangement of calorimeter position. One is a transparent magnet and another is a non-transparent magnet. The transparent magnet, like ATLAS-CS etc., requires high transparency for charged particles passing through. Calorimeters

2023 JINST 18 T06013

are placed outside the detector magnet and therefore the charged particle needs to pass through the coils and its cryostat with a energy loss as small as possible. On the other hand, in non-transparent magnets, like CMS etc., all the particle detectors are generally installed inside the magnet bore except for muon detectors. This results in much larger bore and much longer coil length than those of the transparent magnet.

The common developing item for both type magnets is the conductor, combining both high-strength and low-resistivity Al stabilizer. Conductor development efforts are ongoing in the worldwide projects, CLIC (Compact LInear Collider), ILC (International Linear Collider), FCC-ee(Electron/Positiron Future Circular Collider), FCC-hh(Proton/Proton Future Circular Collider). Other development efforts, like the coil winding, quench protection and over all structural design technologies are also being advanced according to the requirements of detector solenoids. The present status and future prospects of development items are summarized, and the present design status of the magnets for future projects are reported in the latter section.

Table 1. Advances in solenoid magnet technology.

Technology	First Detector of the technology implemented
Al-stabilized superconductor (soldered) and indirect/conduction cooling	ISR [2], CELLO [3]
Secondary winding and quench back	PEP4-TPC [4]
Co-extruded Al-stabilized superconductor	CDF [5]
Inner winding	TOPAZ [6]
Carbon-fiber-reinforced-plastic outer vacuum vessel/wall	VENUS [7]
Thermo-siphon and indirect cooling	ALEPH [8], DELPHI [9]
2-layer coil and grading	ZEUS [10], CLEO [11]
Al-stabilizer w/ Zn, and Isogrid vacuum vessel	SDC-Prototype [12]
Shunted coil w/ conductor soldered to mandrel	CMD-2 [13]
High-strength Al-stabilizer w/ Ni micro-alloying and fast quench propagation w/ pure-Al strips and heater	ATLAS [14]
Hybrid conductor configuration using electron beam welding	CMS [15]
Self-supporting coil with no outer support cylinder	BESS-Polar [16]

2 Technology for detector magnets

Many engineering efforts have been made to improve transparency of the detector solenoids, and modern detector solenoid design concepts have been realized [17].

- A superconducting coil is wound with Nb-Ti/Cu conductor/cable cladded with pure aluminum stabilizer.
- The coil is conduction cooled from cooling pipes set on an outer support cylinder.

2023 JINST 18 T06013

	ATLAS -CS	CMS
Requirement:		
Clear bore rad. (m)	1.18	2.95
Central field (T)	2	4
Design parameters:		
Coil inner rad. (m)	1.23	3.25
– half-length (m)	2.7	6.25
No. of coil layers	1	4
Full thickness (m)	0.045	∼0.3
Max. field (coil) (T)	2.6	4.6
Nom. current (kA)	7.73	20
Stored energy (GJ)	0.04	2.6
Cold mass (t)	5.7	220
E/M (kJ/kg)	7	12.3

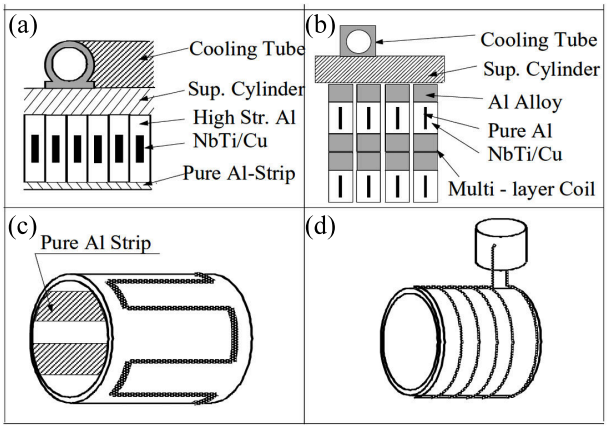

Figure 1. Detector solenoids in LHC. Cross section of ATLAS CS (a) and CMS (b), cooling tube configuration of ATLAS CS (c) and CMS (d). Reproduced with permission from [19].

- No structure (i.e. bobbin) exists inside the coil winding.
- Epoxy based resin is painted or impregnated into the coil winding to integrate winding conductors and the outer support cylinder both mechanically and thermally.

These design concepts give good transparency for the particles passing through, as well as a light cold-mass weight and a simple coil structure. Consequently, coils for non-transparent solenoids have been designed with similar design approaches, too. An overview of the recent developments for the detector solenoids is described below.

2.1 Aluminum stabilized superconductor and superconducting coil

Aluminum stabilization of the superconductor is a key technology in modern detector magnets. It contributes to the stability of the superconductor with minimum weight and high transparency for the particles passing through. The electro-magnetic forces generated in the coil winding are sustained by the conductors themselves in combination with the outer support cylinder. Since pure aluminum stiffness is rather low with a yield strength of about 30 MPa, the outer support cylinder made of aluminum alloy would need to contribute enough mechanical strength to keep the stress in the coil at a reasonable level. This means that reinforcement of conductor saves thickness of the outer support cylinder. Aluminum-stabilized superconducting conductors have benefited from a number of improvements, notably regarding its mechanical strength over the last four decades. The evolution of conductors is summarized in figure 2. One approach has been to provide homogeneous reinforcement of the stabilizer itself; the other was to work with a hybrid configuration of soft high conductivity material with a strong alloy.

Homogeneous reinforcement was established by combining micro-alloying and cold-work hardening. It was found that nickel additive effectively contributes to mechanical strength while keeping a reasonably low electrical resistivity in the aluminum. Figure 3 shows mechanical strength of aluminum stabilizer doped with various metals as a function of electrical resistance at 4.2 K. The figures in parentheses represent the area reduction ratio by cold drawing. It can be seen that the

2023 JINST 18 T06013

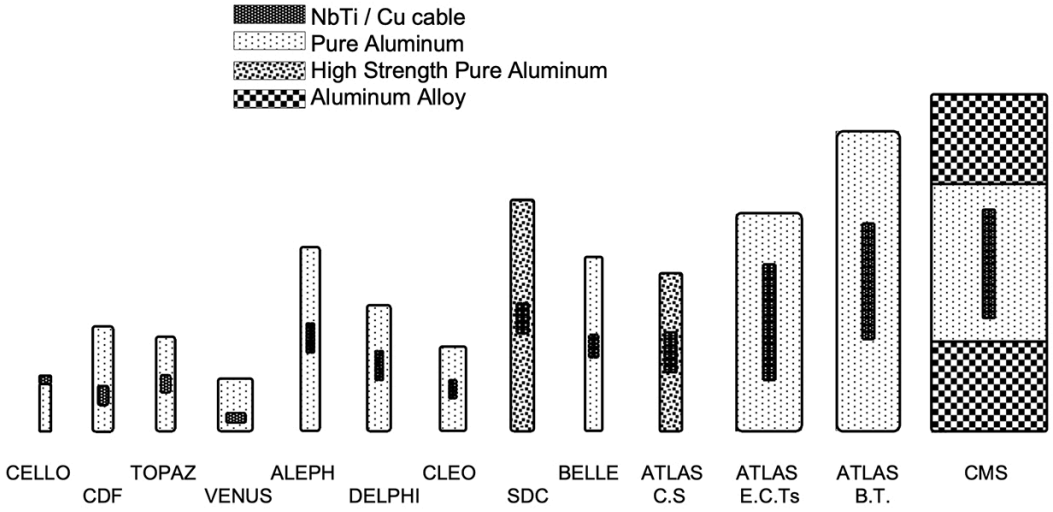

Figure 2. Evolution of conductors for detector magnets. Reproduced with permission from [19].

Table 2. Relevant parameters of high-strength conductors.

Type	Composition	Yield strength (MPa)		RRR
		Al	Full conductor	
ATLAS-CS	Ni(0.5%)Al	110	146	590
CMS	Pure Al & A6082-T6	26 428	258	1400

strength of the aluminum stabilizer is improved by the area reduction due to cold drawing, while its residual resistivity ratio (RRR) is degraded. The ATLAS central solenoid was wound with the conductor clad with reinforced 0.1 % Ni doped aluminum stabilizer, it gives a one-third reduction in the thickness of coil in comparison with a conductor using a pure aluminum stabilizer [18, 19]. A hybrid configuration, which consists of a combination of pure aluminum stabilized superconductor with high strength aluminum alloy (A6082) blocks attached to both sides by electron-beam welding was developed for the CMS solenoid. Such a hybrid configuration is very effective in large-scale conductors because it can be welded. It allows a hoop strain of 0.15 % induced by a hoop stress of 105 MPa, and it is an essential feature of the 4 T CMS solenoid design.

In the hybrid approach the electro-magnetic force acts on the superconductor, which is confined in the soft pure aluminum. In order to ensure that the conductor does not migrate in this medium when it is required to operate at fields greater than 4 T that are being considered for future detectors, it is envisaged to combine the two approaches to reinforcement, co-extruding the conductor with the micro-alloyed material followed by electron beam welding (EBW) of the tough alloy flanges. Table 2 summarizes the relevant parameters of high-strength conductors [19].

2.2 Inner winding technique to support cylinder and indirect/conduction cooling

Solenoid coils have traditionally been wound with tension to the outside of a mandrel/bobbin. The tension should be sufficiently large to ensure compressive pre-stress between the coil-winding and

2023 JINST 18 T06013

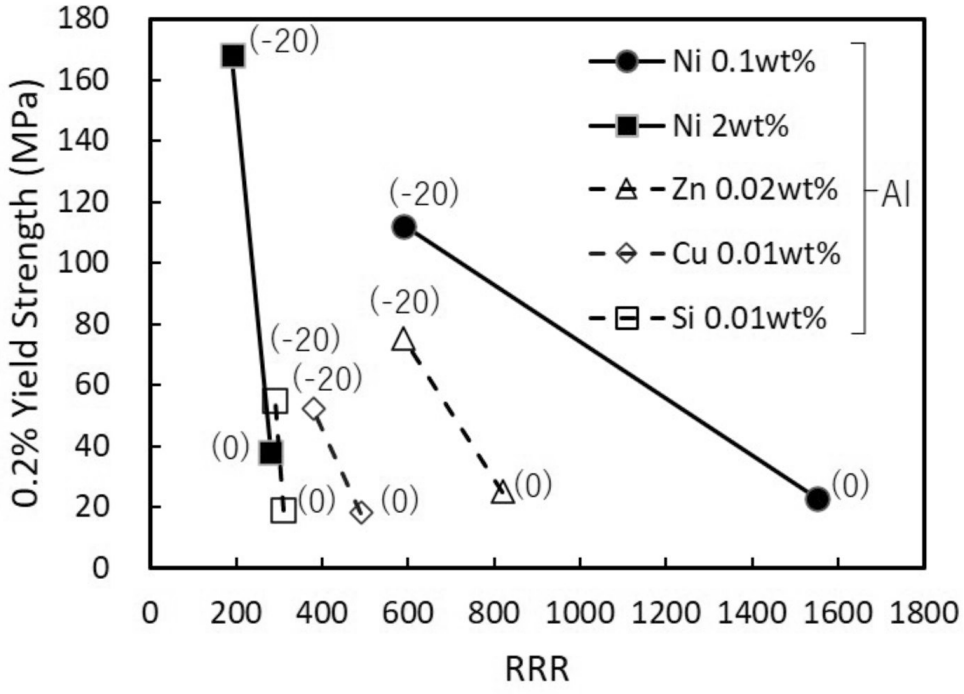

Figure 3. Mechanical strength (0.2 % yield strength) of aluminum stabilizer as a function of RRR. The note of (−20) means area reduction of 20 % by the cold work hardening. The note of wt% means weight %.

inner-bobbin for eliminate the separation of the coil from the inner-bobbin when the hoop stress increases in the conductors according to the coil excitation. This requires the bobbin to be thick enough to avoid buckling. Conversely, if the winding can be done inside a support cylinder then the compressive force further increases when the current is increased. There is no bucking force during the winding. In addition, having the ground insulation between coil and the support cylinder under pressure ensures the good thermal conduction required for indirect cooling from the cooling pipe placed on the outer surface of the support cylinder. LHe flow may be realized by using the force 2 phase helium flow in the cooling pipe attached to the outer support cylinder, or by natural gravitational convention inside the cooling pipe configured for enabling it [1, 9, 10, 13, 14]. As an example, ATLAS-CS winding concept is shown in figure 4.

2.3 Energy/Mass ratio and transparency

Compactness and transparency of the magnet are important in order to create a magnetic field with minimum disturbance for the particles and having maximum detector acceptance. For these reasons, the ratio of stored energy to effective coil cold mass, called the E/M ratio, is a useful parameter to characterize the lightness, and compactness (or efficiency) of the magnet. In the case of a solenoid coil,

$$E/M = \frac{\int \frac{B^2}{2\mu_0} dv}{\rho V_{\text{coil}}} = \frac{\sigma_h}{2\rho}, \tag{2.1}$$

2023 JINST 18 T06013

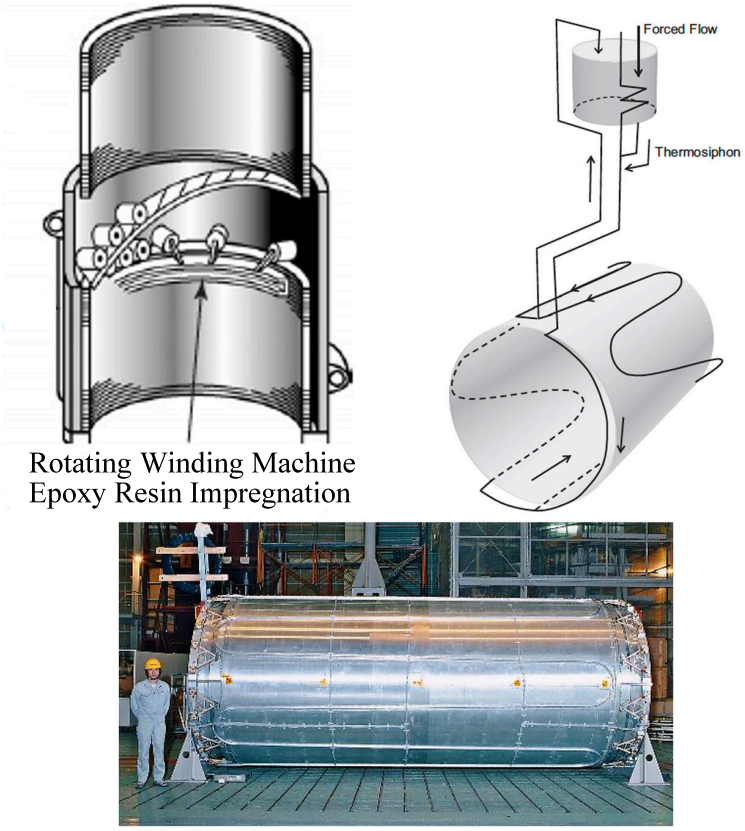

Figure 4. Concepts of inner coil winding and indirect/conduction cooling of the detector solenoid with a photo from the ATLAS-CS support cylinder with cooling pipe.

where σ_h is hoop stress, ρ equivalent coil density. The necessary coil thickness is determined by

$$t = \frac{B^2}{2\mu_0}\frac{1}{\sigma_h}. \tag{2.2}$$

The E/M ratios in various detector solenoids are shown in figure 5 [1, 19]. In early generations of thin solenoids, a typical E/M ratio was $\sim 5\,\mathrm{kJ/kg}$. Based on the development of high strength aluminum stabilizer, a level of $\sim 10\,\mathrm{kJ/kg}$ was achieved for the SDC prototype. Using a further advance high-strength Al-stabilizer, the ATLAS central solenoid realized 8.1 kJ/kg, at it test field v2.1 T for the main/production solenoid with keeping redundant safety margin even in case of the full energy absorption in the case of quench, in the long term serviced operation. The CMS solenoid realized 12 kJ/kg at the nominal field of 4.0 T with a very redundant quench protection system providing reliable energy extraction and limiting the energy absorption into the coil to be partial (around half) energy. In case of the ATLAS magnet system, the quench protection system was designed with quench protection heaters resulting in the full energy absorption in the coil, On the other hand, the quench protection system for the CMS solenoid adopted the energy extraction resistor with redundant circuit breakers, resulting in the reduced energy absorption in the coil. It is interesting that the CMS solenoid realized the higher E/M ratio than that of the ATLAS Central Solenoid. It also provided an additional advantage of the coil physical thickness to be thin, even

2023 JINST 18 T06013

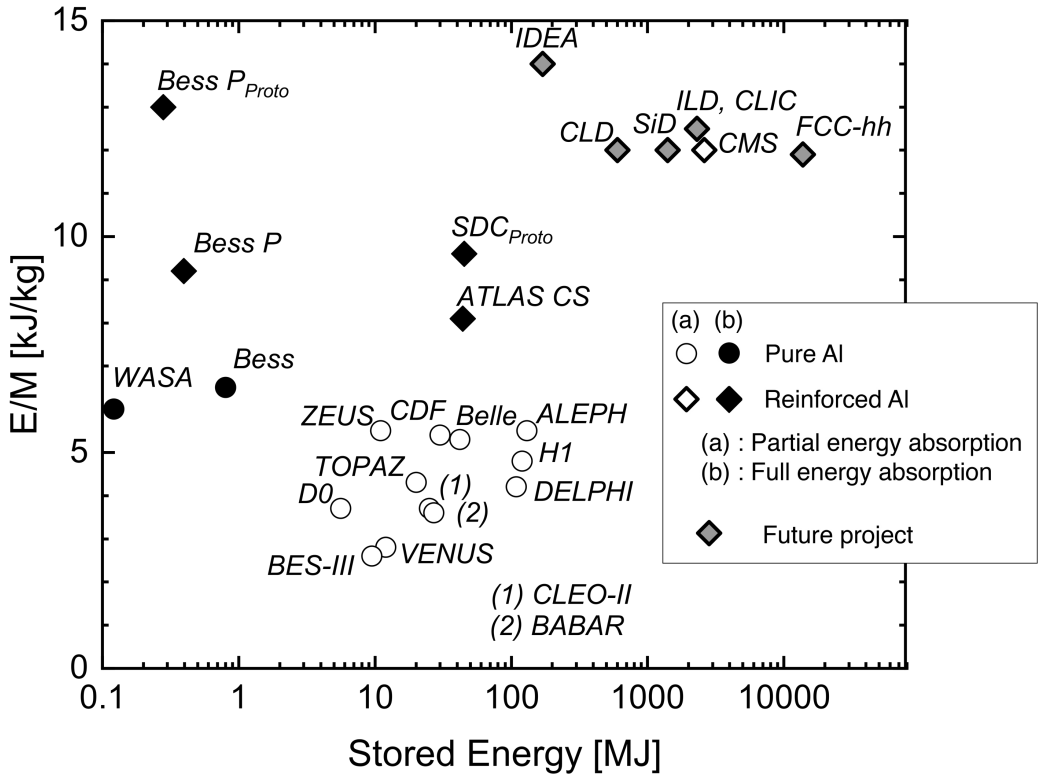

Figure 5. E/M ratio as a function of stored energy. Circle and diamond symbols represent the coil using pure aluminum and high-strength aluminum stabilizer, respectively. Open and closed symbols represent the system with energy extraction resistor realizing partial energy absorption in the coil and the system in which the stored energy is fully dissipated in the magnet. Gray color symbol represents the future projects.

though the transparency was not required. As a record, the BESS polar prototype solenoid realized the E/M ratio also realizing the full energy absorption without the coil damage.

Another limiting factor for the E/M ratio is the quench protection. In the adiabatic condition temperature rise after quench can be expressed as,

$$\int_{t_{\text{quench}}}^{t_{\text{end}}} j^2 dt = \int_{T_0}^{T_{\max}} \frac{C_{p\ \text{ave}}}{\rho_{\text{ave}}} dT, \tag{2.3}$$

where t_{quench} is the time quench occur, t_{end} is the time current is completely down, j is the current density, T_0 is the operation temperature, $T_{\max}$ is the maximum temperature, $C_{p\ \text{ave}}$ is the average volumetric specific heat of the conductor, and the ρ_{ave} is the average electric resistivity of the conductor. The equation indicates that once the conductor material is determined the maximum temperature after quench is proportional to the square of current density times the current discharge time (i.e., the concept so called MIITs) [20]. Since the detector solenoid has large stored energy and also contains sensitive detector electronics in its aperture, the discharge time may not be shortened too much. For the large-scale conduction cooling solenoid, to avoid the excess thermal stress in the structure, it is generally required to limit the maximum temperature to relatively low value less than $\sim$ 150 K. For these reasons the engineering current density of the detector solenoids is generally kept

2023 JINST 18 T06013

low. To achieve the transparent solenoid magnet with such low current density, use of Aluminum stabilizer is essential with its light weight and good electric conductivity.

2.4 Thermal stabilization and fast quench propagation by using pure-Al strips

An effort to improve thermal stabilization and fast quench propagation by using pure-Al strips was proposed to suppress the maximum temperature expected with the MIITs concept described above. It will become further helpful to homogenize the coil temperature in case of the energy extraction system not working, the full stored energy needs to be absorbed with less peak temperature and as uniformly as possible in the coil [16, 17, 21]. This is possible if the quench propagation is much faster than the power decay time during a quench. A technique to increase the quench propagation velocity is to use axial pure-aluminum strips, as the concept shown in figure 6. This idea was implemented and experimentally verified in the development of various thin superconducting solenoids [14, 16, 17].

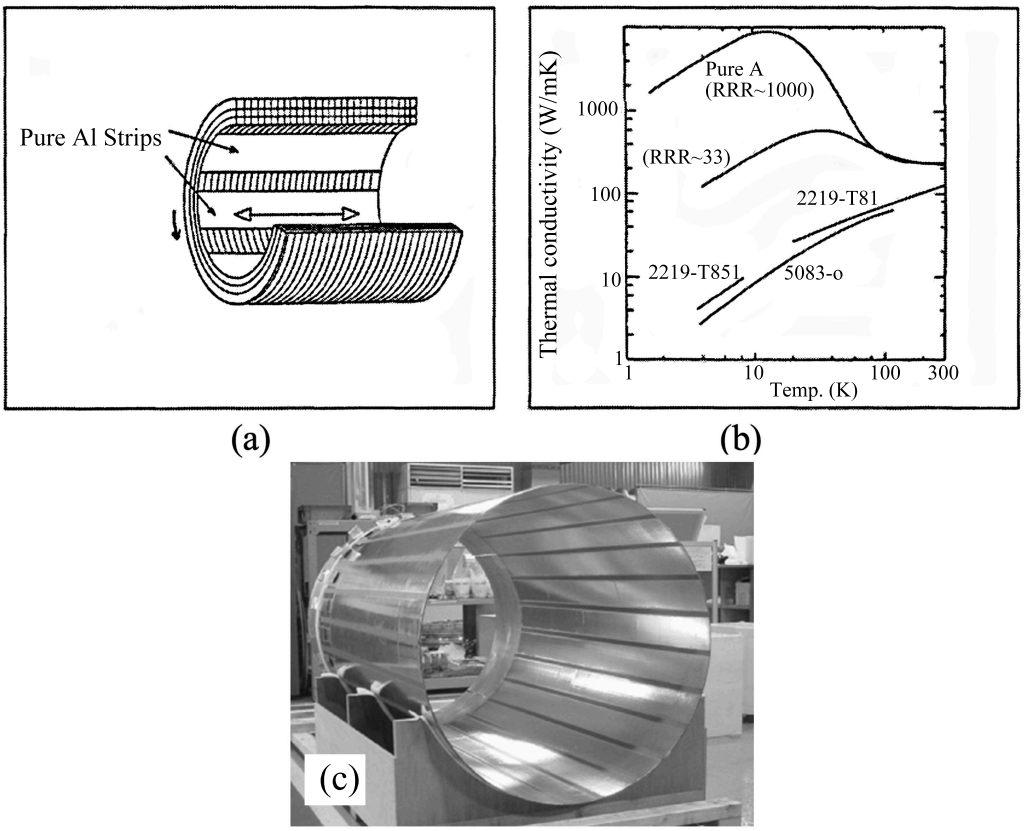

Figure 6. (a) Axial pure-Al strip quench propagator to enhance the effective thermal conductance along the coil axial direction, and (b) thermal conductivity of pure Al strip compared with other materials, (c) photo of coil inner surface covered with pure Al strips along the coil axis for the BESS-Polar solenoid.

If an adiabatic condition was assumed, the longitudinal (along the conductor) quench propagation velocity V_ϕ is given by

$$V_\phi = \frac{j}{C_{p\ \mathrm{ave}}}\sqrt{\frac{L_0 T_s}{T_s - T_0}}, \tag{2.4}$$

2023 JINST 18 T06013

where L_0 is the Lorentz number, T_s is the wave-front temperature. The relative axial (transverse) velocity is given by

$$V_z = \sqrt{\frac{k_z}{k_\phi}} V_\phi, \tag{2.5}$$

where V_z is axial quench velocity, and k_z and k_ϕ are axial and circumferential thermal conductivity, respectively. One sees that V_z may be enhanced by increasing the axial thermal conductivity k_z. Normally, the axial thermal conductivity is suppressed by turn-to-turn electrical insulation made of Kapton (Upilex) and/or glass tap. A pure aluminum strip of 1–2 mm thickness glued on the inner surface of the coil serves to enhance the effective thermal conductivity in the axial direction by bypassing the axial electrical insulation. As shown in figure 6, pure aluminum with RRR $\geq$ 1000 is especially appropriate for this purpose because of its enhanced thermal conductivity around the temperature range in us. At 4.5 K, $k\phi$ is $>$ 2000 W/m·K. With the 1–2 mm thick pure aluminum strip, k_z is estimate to be $\sim$ 100 W/m·K effectively with pure-aluminum strips, while it is 1 W/m·K without. The enhanced quench propagation velocity may be expressed by

$$e = \frac{V_z}{V_\phi} = \sqrt{\frac{k_z}{k_\phi}} \tag{2.6}$$

and one can expect the enhancement of the axial quench propagation by an order of magnitude. In summary, faster axial quench velocity can be expected as improvement of axial thermal conductivity. It may be realized by using pure aluminum strips placed along the coil axial direction on inner surface of the solenoid coil.

2.5 Transparent vacuum vessel

An outer vacuum vessel is a massive wall, because it needs rigidity to withstand buckling forces due to external pressure. In order to minimize the material in the vacuum vessel as well as in the cold mass, a brazed honeycomb vacuum vessel has been investigated for the SDC solenoid at SSC [21, 22]. A major feature of honeycomb plate is the high stiffness, in spite of its light weight. Further, brazed honeycomb panel have the possibility for welding and high reliability due to the fact that no epoxy resin is used. A prototype brazed honeycomb vacuum vessel was fabricated in order to validate the honeycomb vacuum vessel design and to establish the fabrication method. The fabrication steps of a brazed honeycomb vacuum vessel are shown in figure 7. In the bottom photo of figure 7, a flat honeycomb plate is accurately bent by the concept of 4 point bending method.

An alternative transparent vacuum vessel can be composed of aluminum isogrid shell [23]. Aluminum isogrid shells are typically fabricated in steps: the grid pattern is first CNC machined in flat plates, then the flat plates are formed on a press brake into cylindrical sections which are welded to make up the shell, as shown in figure 8 [7, 21]. Table 3 summarizes the transparency comparison among solid, Al-honeycomb, and isogrid outer-vacuum vessel/wall, evaluated in the SSC-SDC detector solenoid R&D work [12]. The X/X_0 represents the normalized radiation length of vessel wall (X) by that of aluminum (X_0). Radiation length is defined by the characteristic amount of matter traversed for these related interactions, frequently defined in the unit of g/cm^2 [17, 24, 25]. The detail explanation of radiation length is explained in the section 34.4.2 of [24], and it is usually used to evaluate and

2023 JINST 18 T06013

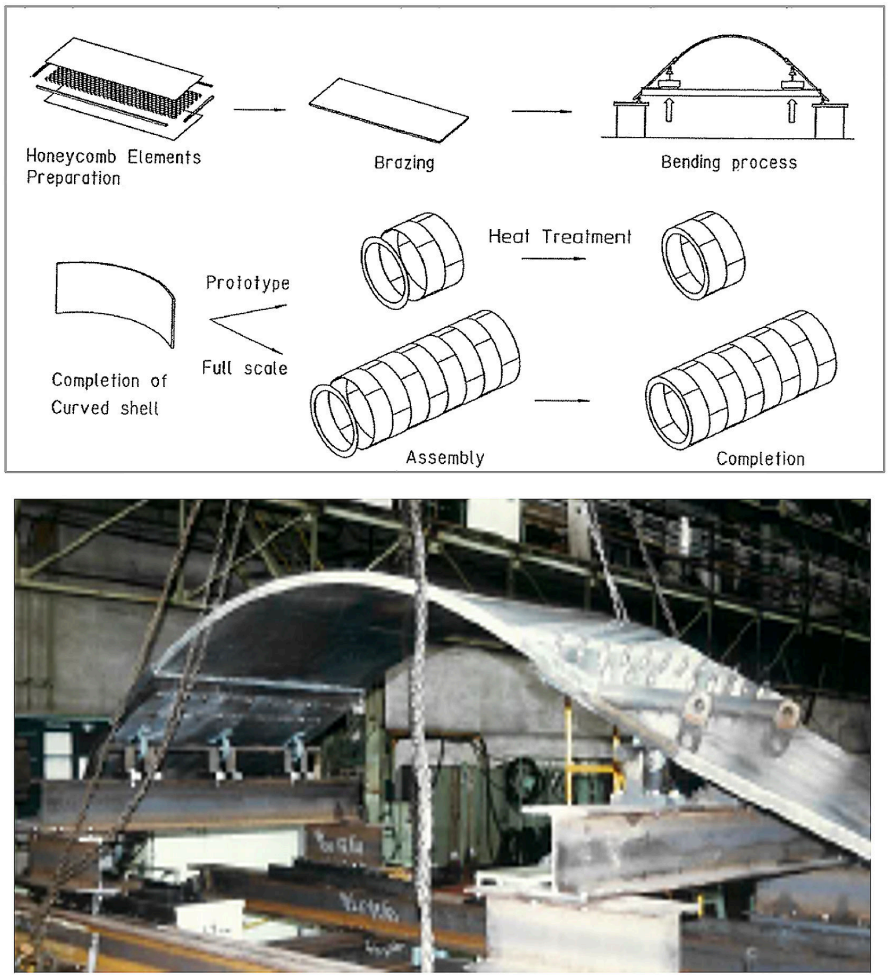

Figure 7. Fabrication steps of a brazed honeycomb vacuum vessel (top), and photo of bending process (bottom).

Table 3. Comparisons of solid, isogrid and honeycomb outer vacuum vessel/wall evaluated for the SSC-SDC detector solenoid design.

Type	Unit	Solid	Isogrid	Honeycomb
Al alloy		5083	5083-H32	6951/4045-T6
Number of shells to be assembled		12	12	21
Physical wall-thickness	mm	27	46	46
Skin wall-thickness	mm	(27)	4.0	3.0+3.0
Effective thickness (averaged)	mm	27	11	7
Weigh reduction ratio		1	0.4	0.26
Normalized radiation thickness of vessel wall by that of aluminum (X/X_0)		0.303	0.123	0.079

compare the transparency for charged particles. The X/X_0 of Al-honeycomb wall was clearly smaller than other two types, so it may realize the best transparency under a normalized safety condition.

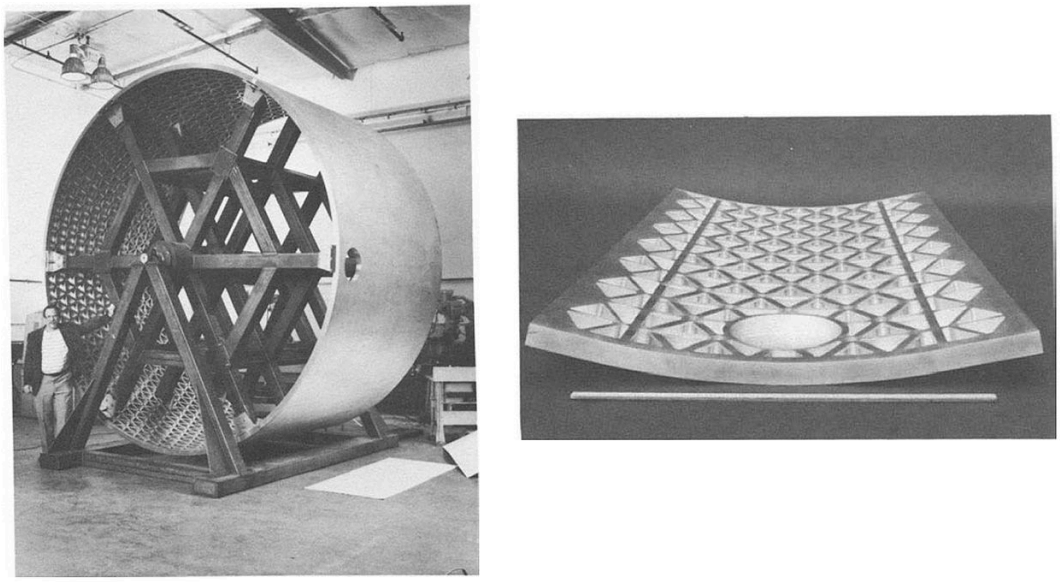

Figure 8. Welded isogrid shell on assembly fixture (left), and isogrid test panel with a hole for cryogenic port.

Although an isogrid shell will not be as thin as a honeycomb shell, it may have various advantages with the well-understood manufacturing process and easier arrangements to adapt cryostat parts, for example, support structure bases or holes for cryogenic ports. Making good use of each advantage, isogrid and honeycomb technologies may be well harmonized to compose a light weight and transparent vacuum vessel. Further effort for an ultimately transparent vacuum vessel/wall has been made by using plastic material such as Carbon/Glass-Fiber-Reinforced-Plastic (CFRP/GFRP). The outer vacuum vessel for the TRISTAN-VENUS detector solenoid was made of 30mm thickness CFRP [7]. Since the reinforced plastic technology advances, the vacuum vessel made of plastic material is considered for future detector solenoids [26, 27].

3 Future prospects for detector solenoid technology

The detector solenoids design study is in progress for future big projects in Japan and Europe, that is, ILC, FCC and CLIC. The proposed design parameters for each solenoid are summarized in table 4.

Table 4. The proposed design parameters for the detector solenoids for future projects.

Projects	Magnet	B_c (T)	InnerR (m)	Length (m)	E/M (kJ/kg)	Stored energy (GJ)
FCC-ee	IDEA	2	2.24	5.8	14	0.17
	CLD	2	4.02	7.2	12	0.6
FCC-hh		4	5	20	11.9	13.8
CLIC		4	3.65	7.8	13	2.3
ILC	ILD	4	3.6	7.35	13	2.3
	SID	5	2.5	5	12	1.4

2023 JINST 18 T06013

The main development item for the future detector solenoid is Al stabilized superconducting cable with both higher strength and keeping high RRR, and most likely solution is the combination of technologies used in the conductors for ATLAS-CS and CMS. The approach adopted in ATLAS-CS conductor is the homogeneous reinforcement of the aluminum stabilizer, that is, to dope Ni into Al stabilizer and to apply cold-work hardening simultaneously. Another approach used in CMS conductor is the reinforcement by using the hybrid configuration with pure-aluminum stabilized conductor and high strength aluminum alloy, which are mechanically bonded by electron beam welding. By combining these two approaches, the (0.2 %) yield strength of more than 300 MPa might be expected as shown in figure 9 [28]. Various conductors are designed in the future projects described in the next section.

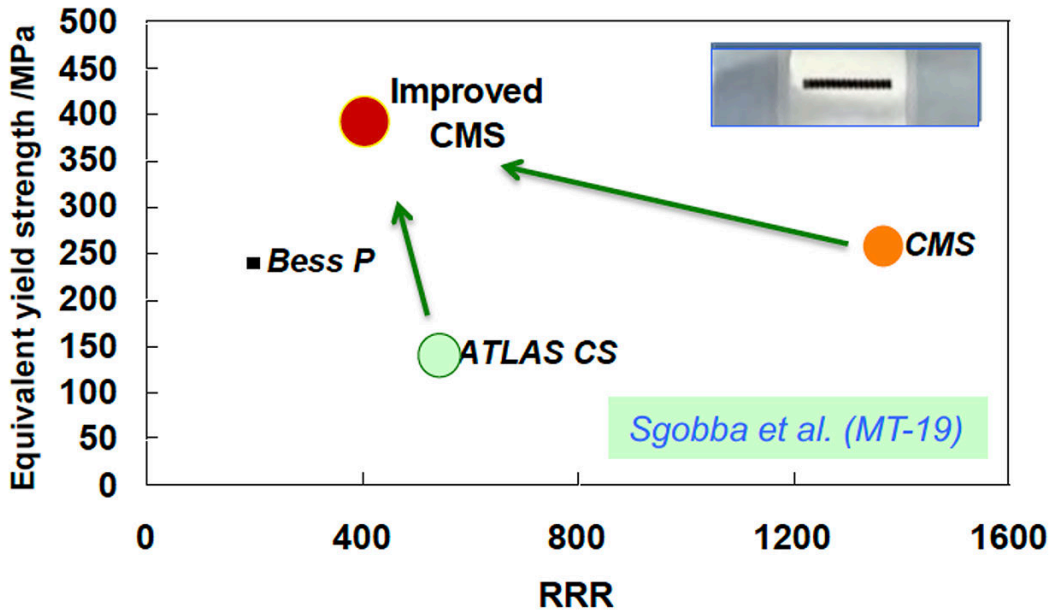

Figure 9. Yield strength and RRR which were realized in ATLAS-CS and CMS. Expected parameters by combining two technologies are also plotted.

The other magnet fabrication technologies will be also developed with the advanced Al-stabilized conductor, and the technologies based on the present ones will be used adaptively for each project; inner coil winding technique inside the outer shell, indirect cooling to reduce materials used in magnet structure, and utilize pure aluminum strips as temperature equalizer in the steady operation and fast quench propagator for the safe quench protection. The vacuum vessel design is one of the important studies especially for the detector solenoid requiring the transparency for the charged particle passing through. The vessel design with rigidity, light-weight and high transparency will be required. The materials used for the vacuum vessel are also interesting topic. The material technology is rapidly developed and options such as plastic composites are of interest [27]. An effort in design and studies for the use of high temperature superconductor are also requested to reach the increasing demand on sustainability in reducing power consumption of our superconducting detector magnets, even for minimizing the cryogenics power consumption. A concern for future large-scale magnet development is to retain and transfer expertise in current technologies as well as

2023 JINST 18 T06013

the technological breakthrough. The technologies described in section 2 have been used successfully for the manufacturing of many superconducting detector magnets in the past four decades thanks to the technical and scientific competencies developed, with many regular breakthroughs. However, the large-scale detector magnets with Al-stabilized conductors have not been fabricated since after the success of CMS and ATLAS-CS in LHC. Unfortunately, conductor manufacturers discontinued to keep the technology to fabricate Al-stabilized conductors nowadays, due to long interval without production order Today complementary efforts are needed to resume again an equivalent level of expertise, to continue the effort on research and to develop these technologies and apply them to each future detector magnet project. Especially, it is mandatory for the development of Al-stabilized conductor to get the industry involved, because only industry has the capacity to manufacture such Aluminum stabilized superconductor, currently. The production will have to be re-established with industrial partner or a specific industrial support. A collaborative framework between institutes and industries is needed, and pre-industrialization programs will be necessary to adapt the technologies to the specific needs of the new detector magnets, and to validate that the required quality and performances can be reached. In addition, quality control and quality assurance are necessary from a long-term perspective to avoid problems that eventually lead to performance degradation and are only discovered after years, such as contamination of a refrigerator system or leaks due to poor quality connections on a cooling circuit, as discovered during long shutdown 1 and long shutdown 2 on the detector magnets. An effort will also have to be made on quality assurance during the design and supply phases with the industrial suppliers to define together and achieve the necessary standards for the detector magnets so that they can operate for decades without risk of performance degradation. In the discussion above, a major topic of discussion is a solenoid-shaped magnet as a detector solenoid. Other types of magnets, such as split coil and saddle shape coil, could be candidates depending on the requirements from a physics viewpoint [29]. The continuous effort of coil design study is important to make an magnet design optimized for experimental goals. The detector solenoid for mid-scale experiment sometimes uses a conventional Cu-stabilized Nb-Ti conductor. The conventional solenoids for such experiments do not need the development of unique conductor, but instead, precise control of magnetic field distribution might be required. The development efforts are on-going in terms of the magnetic field design technology with high precision simulation, the coil fabrication technology to achieve the design requirement and the control method of magnetic field distribution [30].

4 Future projects

4.1 Detectors for high energy physics

4.1.1 FCC-ee

The Future Circular Collider (FCC) is a project proposed to start after the Large Hadron Collider (LHC) at the European Organization for Nuclear Research (CERN) [31–33]. FCC is a circular particle accelerator with a circumference of 100 km and a proposed center-of-mass energy of 100 TeV in case of proton-proton collisions, which would be FCC-hh. However, the first stage of the FCC is foreseen to be the FCC electron-positron collider (FCC-ee) that can be used to study the electroweak sector with unprecedented accuracy [34]. At the moment of writing this, there

2023 JINST 18 T06013

are three detector designs for FCC-ee: the Innovative Detector for Electron-positron Accelerators (IDEA [35]), the CLIC-Like Detector (CLD [36]) and a design comparable to the IDEA detector that remains to be named. Each of these three designs includes a superconducting solenoid that produces a 2 T magnetic field in the center of each detector. The CLD magnet is positioned outside of the calorimeter volume while the two other solenoids are situated inside the calorimeter barrels just after the tracking detectors. Since the latest (nameless) detector design and its solenoid are still work in process, the following text will focus on the IDEA and CLD magnets.

Figure 10 shows the magnetic flux density as a function of the location in the axisymmetric plane of the CLD and the IDEA detector designs, where the locations of the different sub-detectors are indicated as well. Figure 10 also highlights the most important difference between the two detector designs, which is the location of the solenoid with respect to the calorimeters. Since the IDEA magnet is inside the calorimeter volume there are strict requirements on the particle transparency that needs to be lower than $X/X_0 = 1$. The concept of the solenoid of the IDEA is similar to the ATLAS Central Solenoid [37] and whereas the CLD magnet is similar to the CMS solenoid [38]. However, in terms stored energy and free-bore diameter there are some important differences. The free-bore diameter of the IDEA solenoid is 4.2 m and is almost two times bigger than the free bore of the ATLAS CS. This also means that the IDEA magnet has around four times the stored magnetic energy of the ATLAS CS at 170 MJ. The free-bore diameter of CMS is 6 m with a stored energy of 2.6 GJ. The CLD design has a larger free bore of 7.2 m and its stored energy is 600 MJ. This results in the design parameters for the IDEA and the CLD summarized in table 5 [39].

To highlight the challenges of the IDEA and CLD designs the energy density, i.e., the stored magnetic energy divided by the cold mass weight, can be used as an indication. The ATLAS CS has a maximum energy density of 7.0 kJ/kg during nominal operation (with a demonstrated maximum of 8.1 kJ/kg) while for the IDEA magnet the energy density would be twice as high at 14 kJ/kg. Similarly, the CMS energy density is 11 kJ/kg and the CLD magnet has an energy density of 12 kJ/kg. For reference, the highest energy density ever produced in a detector magnet was 13 kJ/kg in BESS experiment [40]. These high energy densities mean that quench protection needs to be both active and passive in case of a quench detection failure, as well as redundant. The large free-bores in combination with the high stored energies translate to strong requirements on mechanical support and strength of the materials used, especially in the case of the IDEA magnet that is not only very large but the cold mass is extremely thin at only 53 mm [39].

Starting with the mechanical support, both the IDEA and the CLD include an aluminum 5083 support cylinder surrounding the coil windings [39]. The yield strength of Al5083 is higher than 209 MPa at 4.2 K [41]. The aluminum stabilized conductor proposed for these magnets has a yield strength of 147 MPa at 4.2 K when taking the Nb-Ti into account [37]. The conductor will be glued on the inside of the support cylinder with an epoxy resin type adhesive. These can have a shear strength of up to 76.8 MPa at 77 K depending on the type of resin used [42]. Initial mechanical simulations reveal that the IDEA magnet has a peak hoop stress of 105 MPa and for CLD is 75 MPa [39]. Both these values are within the elastic regime of the conductor and the Al5083 support cylinder. The peak tensile strains for IDEA and CLD are 0.13 % and 0.11 %, respectively. At the interface between the coil windings and the support cylinder the peak shear stresses are 0.5 MPa for IDEA and 0.24 MPa for CLD, which is well within the maximum shear stress that adhesives can tolerate. Large scale detector magnets like the IDEA and CLD are only built once and there are usually no representative

2023 JINST 18 T06013

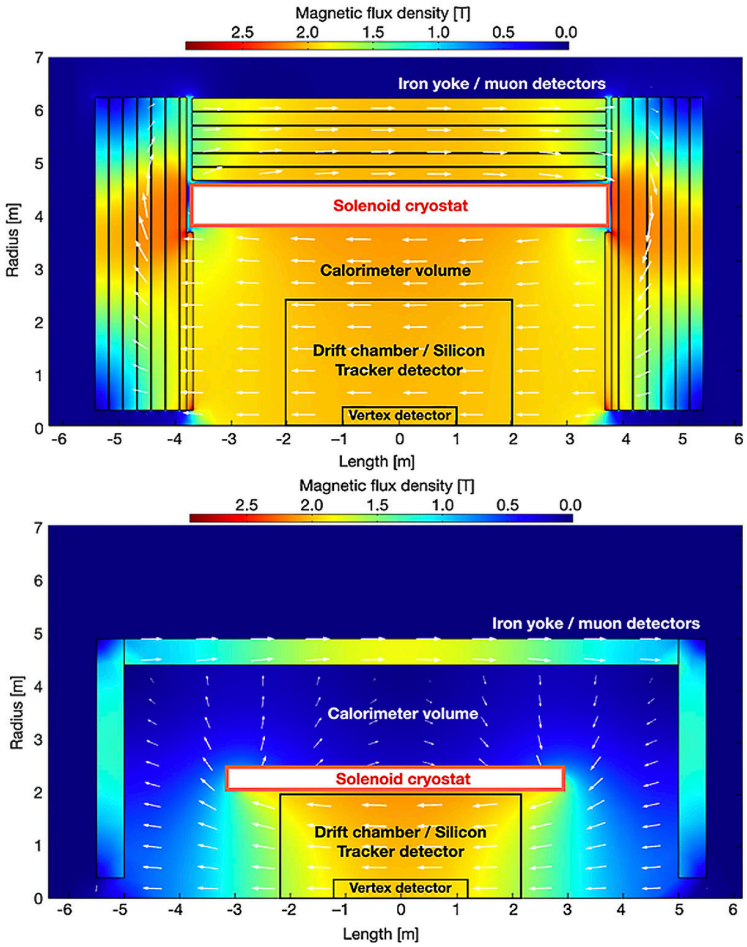

Figure 10. Magnetic flux density as a function of location in the axisymmetric plane of the CLD (TOP) and the IDEA (Bottom) detector designs.

prototypes. Furthermore, because they are in between different particle detectors it is not possible to replace them in they break down. Therefore, it is crucial to have redundant quench protection, even allowing for the case where quench detection fails. An example of the energy extraction layout during a quench is shown in figure 11. Quench simulations for the CLD magnet showed that with an extraction resistor or Run-Down Unit (RDU) the peak temperature after a quench is 60 K and the magnet is fully discharged after 600 s [39].

The IDEA solenoid has a larger energy density, a smaller wall thickness and higher stresses than the CLD magnet [39]. Therefore, a fully three-dimensional simulation of the IDEA magnet was used to study quench protection measures. In addition to an RDU, quench heaters and high purity aluminum (RRR = 3000) quench propagation strips (QP strips) were studied. These QP strips are found in the ATLAS CS as well [37]. The results of 3D simulations for different quench scenarios are shown in figure 12 [39]. The cases with an RDU have the lowest hot-spot temperature equal to 65 K. In all other quench scenarios without a protection resistor, the QP strips have a large effect on the peak temperature. In some cases with QP strips, the peak temperature is decreased by more than 100 K compared to the case when the aluminum strips were not present. In addition, in cases with

2023 JINST 18 T06013

Table 5. Design parameters of the superconducting solenoids for the IDEA and CLD detector concepts at the FCC-ee.

Property	IDEA	CLD	Unit
Conductor			
Conductor material	Nb-Ti/Cu in Al/Ni cladding		
Conductor height	36	36	mm
Conductor width	10	22	mm
Turn-to-turn insulation	1	1	mm
Number of strands	30	26	
Strand diameter	1.1		mm
Cu:SC ratio	1: 1		
Operating current	20		kA
Operating temperature	4.5		K
Coil			
Inner radius	2.235	4.02	m
Length	5.8	7.2	m
Weight	12.5	49.5	t
Number of turns x layers	530 x 1	300 x 1	
Support cylinder thickness	12	25	mm
Total coil thickness	53	102	mm
Central field	2		T
Stored energy	170	600	MJ
Energy density	14	12	kJ/kg

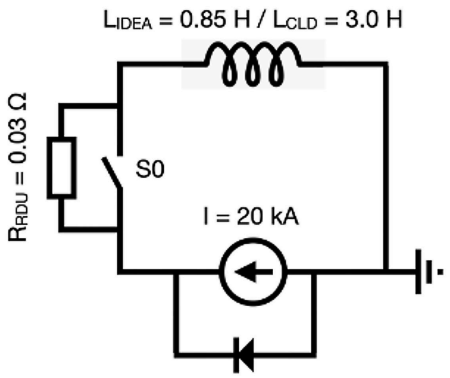

Figure 11. Example of the energy extraction circuit during quench.

QP strips, sixteen turns quench before the quench is detected while in the case without QP strips only eleven turns quench before the quench is detected. This means that the quench propagation strips have a large benefit in terms of quench protection. A benefit of the quench protection strips is that they are fully passive and they even work in case the quench was not detected by the safety systems.

In the previous paragraphs preliminary studies on the FCC-ee detector magnets are described. One of the future problems for detector magnets is the availability of the aluminum stabilized

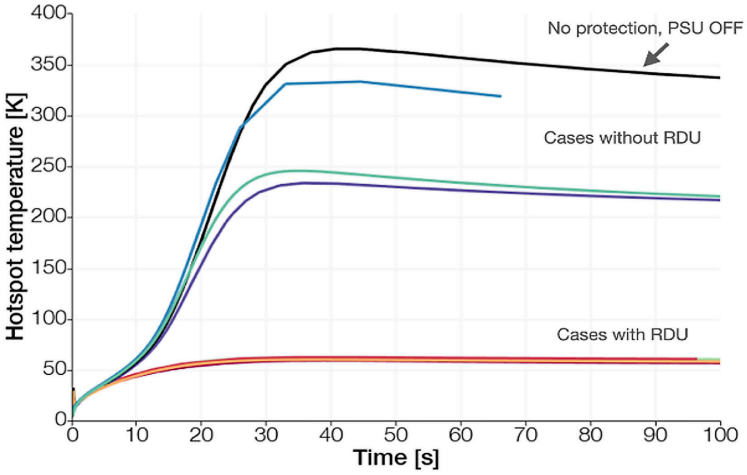

Figure 12. Results of 3D simulations for different quench scenarios.

conductor that is also needed for FCC-ee detector magnets. In addition, the mechanical support, a more detailed quench analysis, the service lines, cryogenics and the cryostat, magnet operation and control are among other topics that still need to be researched and developed in the coming years to enable the construction of these very challenging superconducting solenoids.

4.1.2 FCC-hh

The FCC-hh project foresees a significant 7-fold increase in the particle collision energy with respect to the LHC, and to measure the momentum of the highly energetic collision products with sufficient resolution much more powerful detector magnets are needed as well [43].

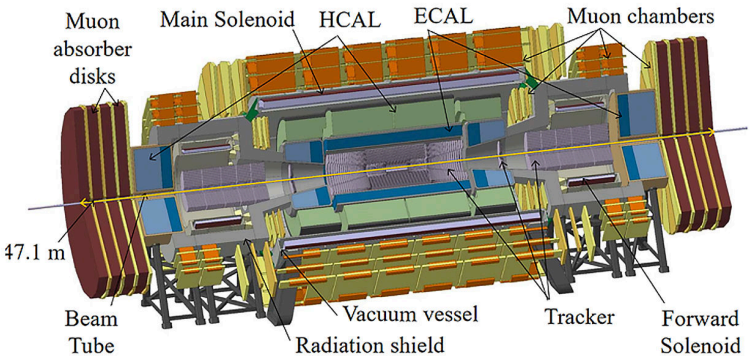

Figure 13. Proposed FCC-hh detector base-line layout.

For this purpose, the FCC-hh detector magnet layout (figure 13) was proposed, featuring three powerful superconducting solenoids (figure 13 and figure 14) each generating 4 T in their bore [44]. Here the central solenoid features are free bore diameter of 10 m and a length of 20 m, whereas the forward solenoids features are a cold mass length of 3.4 m and a free bore diameter of about 5 m. This detector layout has some similarity to the CMS detector, featuring a tracker, electro-magnetic calorimeter (E-CAL), and a hadron calorimeter (H-CAL) in the bore of the magnet, and muon

2023 JINST 18 T06013

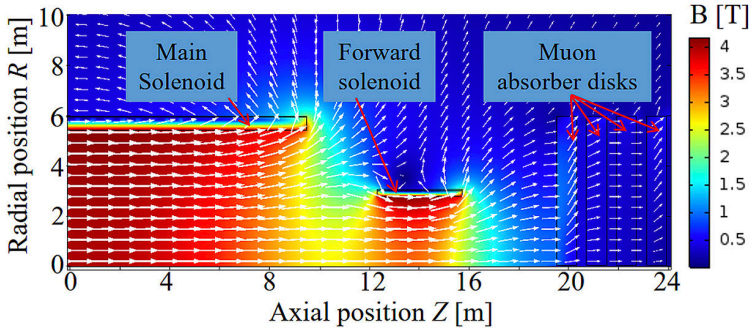

Figure 14. Magnetic field map of the proposed FCC-hh baseline detector magnet configuration.

chambers on the outside of the magnet. The muon chambers utilize the magnetic return flux generated by the main solenoid for the purpose of muon tagging. Unlike CMS, the FCC-hh detector does not feature iron yokes. The unique combination of a main and forward solenoids is proposed to enhance the momentum resolution for particles travelling nearly parallel to the bore tube, and for this purpose trackers and calorimeters are located both in the main and the forward solenoids (figure 13). Due to the close proximity of the main and forward solenoids, the forward solenoids are each exposed to a net attractive force of 60 MN towards the main solenoid. This force is transferred to the solenoid vacuum vessels through reinforced tie rods, and the force is subsequently transferred to the main solenoid through the vacuum vessels and additional support structure.

Table 6. Overview of various detector magnet properties for the FCC-hh proposed detector magnet concept.

Property	Value
Total stored energy (GJ)	13.8
Operating current (kA)	30.0
Combined inductance (H)	30.7
Inductance main solenoid (H)	27.7
Inductance forward solenoid (H)	0.93
Mutual inductance, main-to-forward (H)	0.29
Mutual inductance, forward-to-main (H)	0.001
Cold mass main solenoid (t)	1070
Cold mass forward solenoid (t)	48
Vacuum vessel main solenoid (t)	875
Vacuum vessel forward solenoid (t)	32
Average energy density (kJ/kg)	11.85
Minimum shaft diameter (m)	13

Table 6 shows various properties of the proposed superconducting detector magnets for FCC-hh. The bore magnetic field of 4 T and the energy density of 11.85 kJ/kg are a bit higher than in CMS, while the total stored magnetic energy of 13.8 GJ is more than five times higher. The peak Von Mises stresses in both the main and the forward solenoids are at 100 MPa under nominal conditions which illustrates that, similar to CMS and the ATLAS Central Solenoid, a reinforced conductor is required

2023 JINST 18 T06013

to handle the Lorenz forces. Figure 15 shows the proposed conductor geometry. The main and forward solenoids feature 8 and 6 layers respectively. The conductors comprise Nb-Ti/Cu Rutherford cables surrounded by nickel-doped aluminum stabilizer. The Nb-Ti/Cu Rutherford cables feature 40 strands with a diameter of 1.5 mm, a Cu:non-Cu ratio of 1:1, and a current sharing temperature of 6.5 K. The operating current is 30 kA.

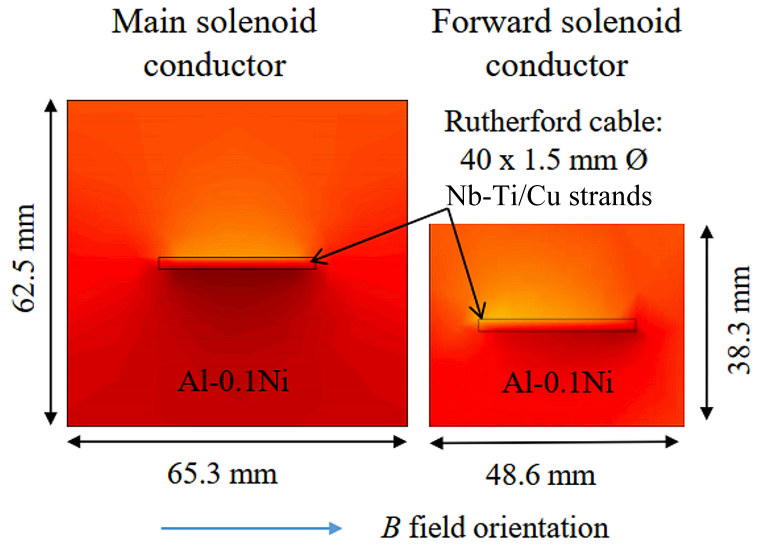

Figure 15. Proposed conductor geometry, featuring nickel-doped aluminum-stabilized Nb-Ti/Cu Rutherford cables.

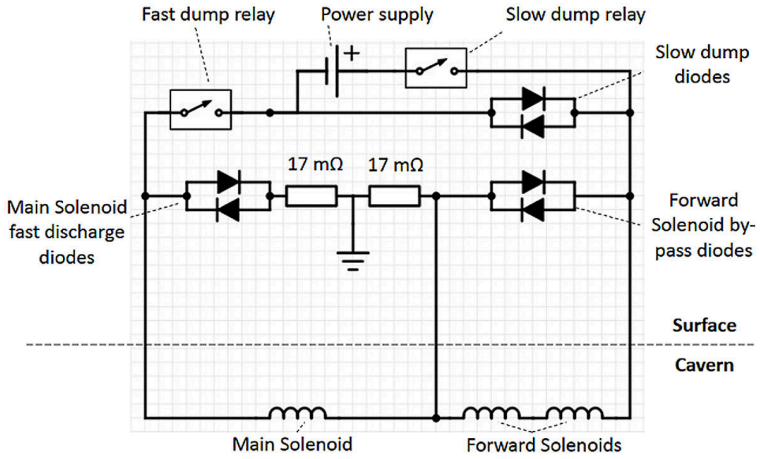

Figure 16. Proposed circuit layout for powering and discharging the FCC-hh detector solenoids.

To power the solenoids, and initiate slow and fast discharges are needed, a combined circuit is proposed (figure 16). The solenoids are powered in series so that a single power supply and slow dump circuit are sufficient to charge and discharge the solenoids. In case of a quench, the different operating current densities in the main and forward solenoids necessitate a current decoupling of these two different magnet types, and therefore the two magnet types feature their own fast-discharging dump

2023 JINST 18 T06013

system comprising diodes and resistors. Moreover, in case of a quench, normal zones are induced in various spots on the solenoids through quench heaters to quickly bring them to the normal state, thus avoiding strong temperature gradients even under fault conditions where the fast dump units fail to discharge the magnets. Thus, this proposed protection scheme provides redundant protection. The calculated peak hot-spot temperature is well below 100 K under nominal conditions (figure 17).

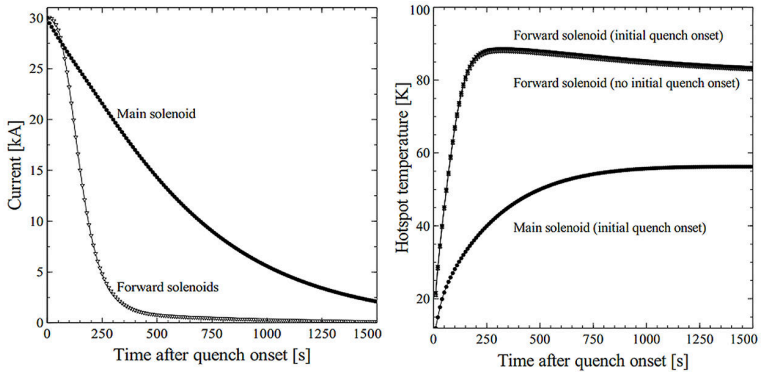

Figure 17. Simulated current discharge and hot-spot temperature development in case of a quench.

In summary, a conceptual design of superconducting detector solenoids was previously developed for the FCC-hh detector [44]. The bore magnetic field, energy density, and mechanical stress are similar to CMS, but the stored magnetic energy and the overall cold mass are more than five times larger. This necessitates the use of mechanically reinforced aluminum-stabilized conductors to handle the Lorentz forces. A particular feature of the FCC-hh detector is the combination of three solenoids which give superior performance for particle tracking albeit at the cost of additional complexity and a large net force of 60 MN on each of the two forward solenoids.

4.1.3 CLIC

The Compact Linear Collider (CLIC) detector project Collaboration [45, 46] intends to build the CLICdet, the new CLIC detector model that has been updated after the CLIC Conceptual Design Report (CDR) was published [36], a detector with a 4 T solenoid magnet operated at the three stages of the CLIC accelerator phases with center-of-mass energies of 380 GeV, 1.5 TeV, and 3 TeV. A view of the detector cross section in the interaction region is shown in figure 18. The feasibility of having a dual beam delivery system serving two interaction regions for the Compact Linear Collider has recently been studied and looks promising for physics programs [47]. At this present stage, no distinction has been made on the magnets for these two detectors. It is the CLICdet baseline magnet design that has been considered with two crossing angles to check the physics feasibility in the interaction regions with the CLIC dual beam delivery system.

The CLICdet magnet design is based on the designs and manufacturing breakthroughs of the CMS solenoid [48] and the Atlas Central Solenoid (CS) [49]. The CLICdet magnet is a 4-T solenoid with 4 layers of superconductor. The main parameters are indicated in table 7. The coil is shorter compared to the CMS solenoid, but it has a larger radius, which gives a total magnetic flux that is about 45 % higher. A 3D view is presented in figure 19. The conductor comprises a superconducting Rutherford cable composed of 32 Nb-Ti strands that is stabilized with an aluminum sheath. This is

2023 JINST 18 T06013

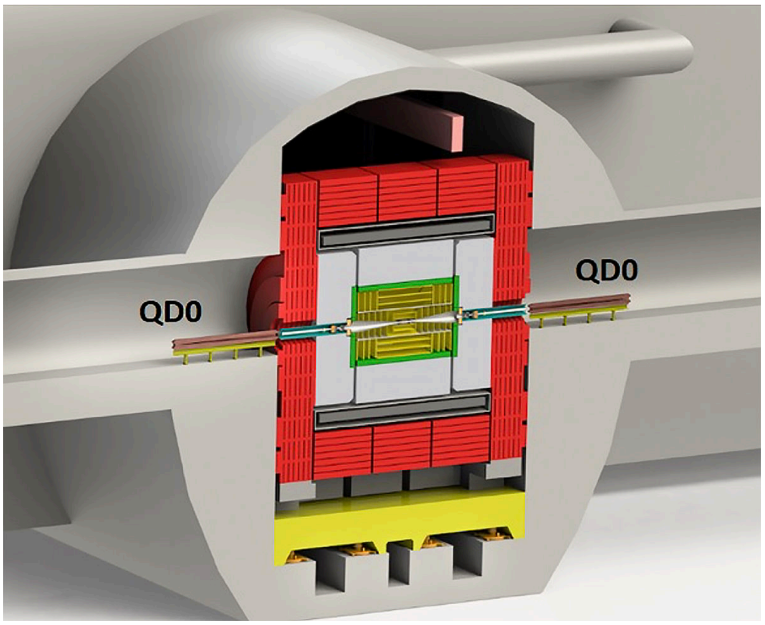

Figure 18. Vertical cut through of the CLICdet detector model showing the QD0 final focusing quadrupole positions outside the detector.

quite comparable to CMS, with a bit larger conductor. The conductor will have to be reinforced to accommodate large magnetic forces applied to the winding. Both options of ATLAS CS and CMS for a reinforced conductor are considered at this stage, respectively the structural cold worked Ni-doped aluminum stabilizer [18] and the Electron-Beam welded aluminum alloy reinforcement [41]. For both options the Rutherford Nb-Ti superconducting cable will be co-extruded with the high RRR aluminum stabilizer. Feasibility programs were led on the structural doped aluminum with a large cross section [51]. Other studies of reinforcement proposed ways to increase the mechanical properties of the conductor, based on the ATLAS CS and CMS reinforcement concepts [28, 52].

Table 7. CLICdet magnet parameters.

Property	Value
Magnetic field at IP (T)	4
Inductance (H)	12
Nominal current (kA)	20
Stored energy (GJ)	2.3
Average energy density (kJ/kg)	13
SC cable number of Nb-Ti strands	32
Conductor cross section (mm^2)	83×20
Coil inner radius (mm)	3650
Coil length (mm)	7800

The magnet will be inside a cryostat supported by the central barrel yoke, similar to CMS. The CLICdet coil will be built using the inner winding technique inside a 50 mm thick external

2023 JINST 18 T06013

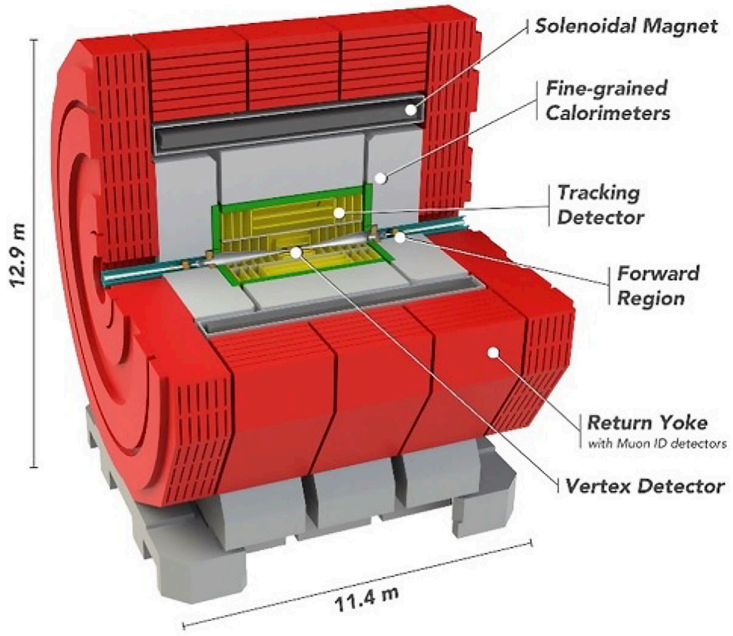

Figure 19. 3-D view of the CLICdet model with external dimensions and cut-out showing the main sub-systems.

mandrel serving as structural external wall, as support for the liquid helium cooling circuit, and as fixation for the supporting tie rods. Similar to CMS, the external mandrel is made from an aluminum alloy of the 5083 grade. It is also used for the protection of the coil against the quench acting as a so-called quench-back cylinder. Aluminum thermal strips shall be used to ensure a good temperature uniformity in the cold mass, during cool down, operation at 4 K, warm-up and for quench protection. Quench heaters are also proposed. The coil will be built from 3 modules with splices integrated in the low field region on the outer radius of the coil, similar to the CMS coil [53, 54]. The vacuum impregnation technique is considered. Heat radiation shields, together with an indirectly cooling with boiling helium at 1.2 bar and in thermosiphon mode will allow the operation of the magnet at 4 K. The CLICdet detector has an iron yoke used to confine the magnetic flux and take benefit of it for the muon detectors installed in between the iron layers. A set of 4 end coils are attached on each end cap of the detector. The cross section of the magnet is given in figure 20. The end coils are used both to limit the magnetic field in the machine detector interface region, as seen in figure 21, in particular on the QD0 final focusing quadrupoles located just in front of the end caps, and to limit the stray field outside the detector to 16 mT at a radial distance of 15 m in the service cavern that is used for detector maintenance and where detector services, powering systems and cryogenics are located (figure 22). The use of these ring coils also contributes to limit the amount of iron in the yoke. It was proposed in the CLIC CDR [55] to build these end coils with normal conducting windings operated at room temperature and water cooled, but we see here a good application of more sustainable solutions in order to limit the heat losses due to the dissipated power by using high temperature superconductor coils, connected in series.

Several technology R&D and pre-industrialization programs will be needed before launching the manufacturing of such a magnet. Power leads [56, 57] and superconducting busbars [58, 59]

2023 JINST 18 T06013

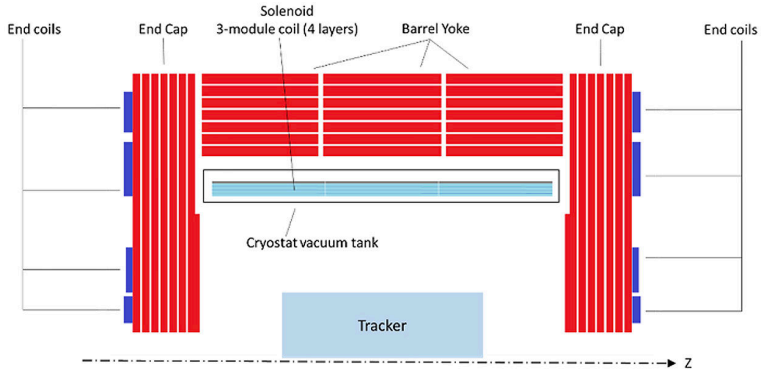

Figure 20. Schematic RZ view of the CLICdet magnet. Only one half of the magnet section along its axis is shown and calorimeters as well as other detector details are not represented.

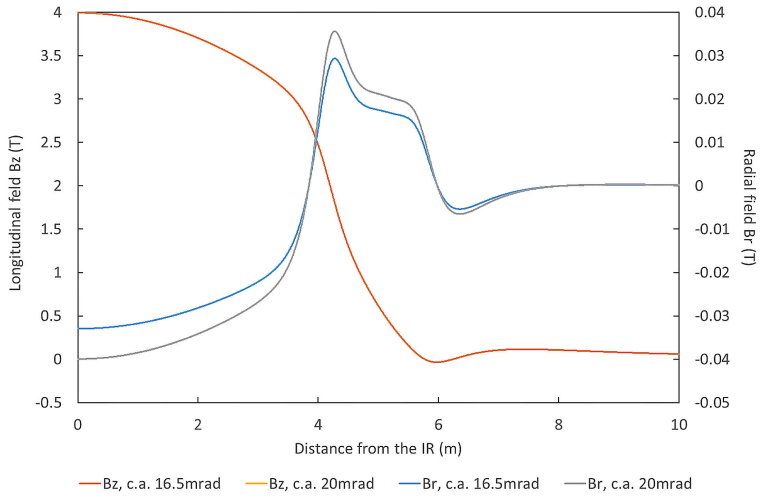

Figure 21. The radial Br and the longitudinal Bz magnetic fields from the IR up to 10m along the beam axis.

are typical applications that can be developed using high temperature superconductors. Other developments can also be performed for powering DC converters and dumping circuit. Dedicated studies applied to the detector magnet applications will be needed. Specific equipment and tooling for the conductor and coil manufacturing (cabling machine, cable brushing and preheating, co-extrusion dies, continuous welding, winding, etc.) and quality control and measurement devices (e.g. continuous quality control of the superconductor, impregnation quality, field mapping) will have to be adapted or re-developed specifically ahead of this project during a pre-industrialization program.

4.1.4 ILD

The design parameters of the magnet for the International Large Detector (ILD), as shown in figure 23, feature a central field of up to 4 T, in a volume of about 275 m^3 (useful diameter 6.88 m over a length of 7.35 m) and its conceptual design has been undertaken by CEA, DESY and CERN [60–62]. The ILD magnet design is very similar to the one of CMS, except for its geometrical dimensions, and the presence of the anti-DID. Consequently, many technical solutions successfully used for

2023 JINST 18 T06013

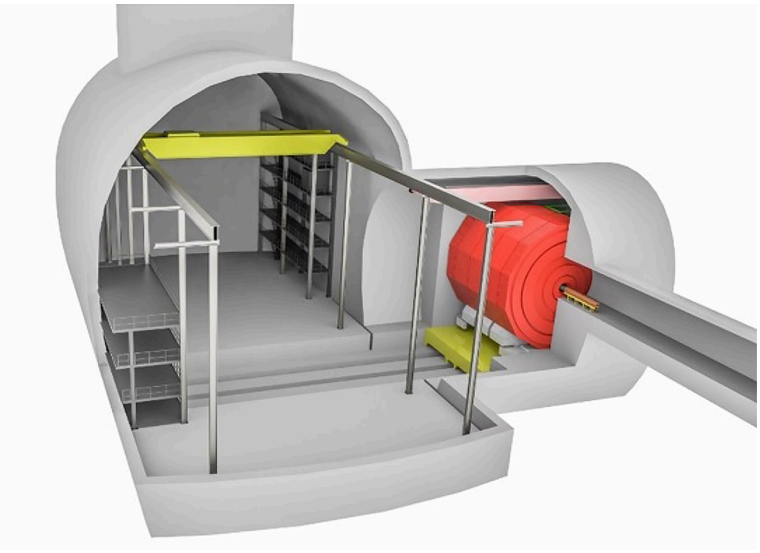

Figure 22. Schematic view of the infrastructure layout in the experimental underground cavern.

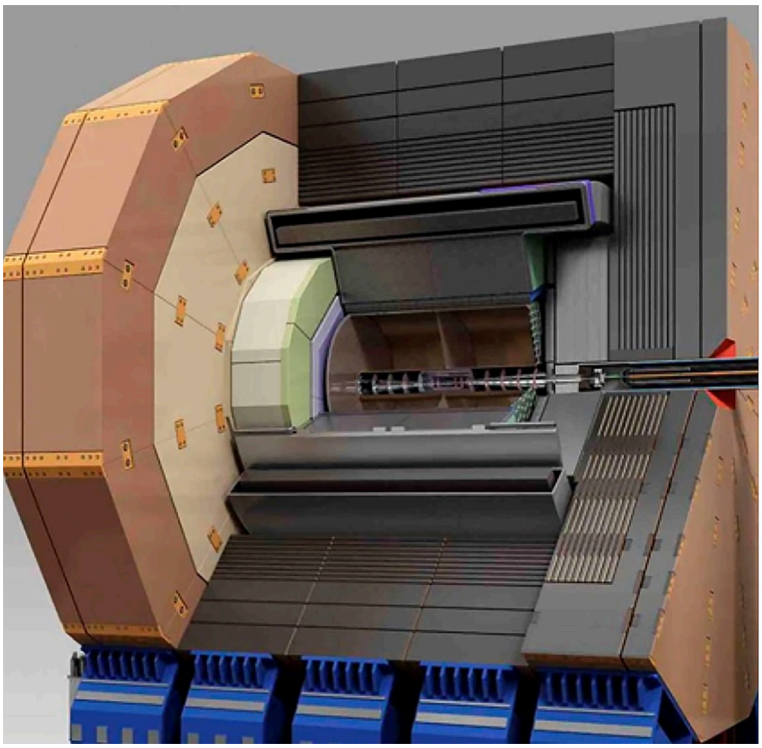

Figure 23. Configuration of ILD.

CMS are proposed for the design of the ILD magnet. The winding radius (3.615 m) of the ILD has larger solid angle than that of CMS (3.25 m). Similarly to CMS, a 4-layer coil is retained, with a nominal current in the range of 20 kA, so the conductor for the ILD magnet has larger cross section of $74.3 \times 22.8\,\mathrm{mm}^2$. It consists of a superconducting Rutherford cable, clad in a stabilizer and

2023 JINST 18 T06013

mechanically reinforced. Two solutions are considered for the reinforcement. The first option is a micro-alloyed material such as the ATLAS central solenoid [14], which acts both as a stabilizer and a mechanical reinforcement. A R&D program on the Al-0.1wt%Ni stabilizer has been launched at CERN and is underway to demonstrate the feasibility of producing a large conductor cross section with this material. The second option is a CMS-type conductor with two aluminum alloy profiles welded by electron beam to the central conductor stabilized with high purity aluminum. These two options are shown in figure 24, together with the actual CMS conductor for comparison.

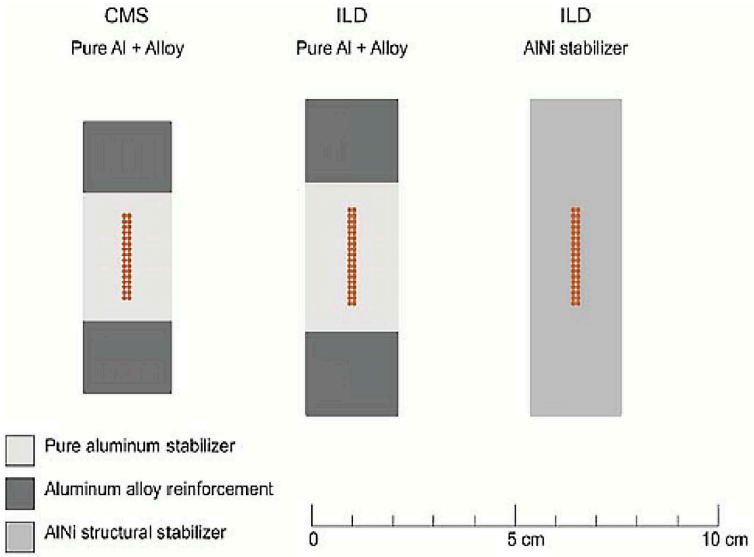

Figure 24. Two options of ILD conductor composition.

4.1.5 SID

A conceptual design study for a 5 T superconducting solenoid for the Silicon Detector (SiD as shown in figure 25) of the International Linear Collider (ILC) has been undertaken at FNAL [63–65]. The solenoid has a clear bore of 5.0 m in diameter and 5.0 m in length, where 5 T magnetic field is produced for inner detectors. Although the winding radius (2.65 m) of the SiD coil is smaller than that of the CMS (2.95 m), it has larger figure-of-merit of 62.5 T^2m than the value of CMS (47.2 T^2m) due to its higher magnetic field. Utilizing the existing CMS magnet conductor as the starting point, a winding design has been proposed for the magnet as shown in figure 26. Finite element analysis shows the resulting magnetic stresses in the coil parts do not greatly extrapolate beyond those of CMS. Major R&D subject for SiD magnet is its conductor required to sustain such large EMF in the coil. In "SiD Letter of Intent" described in 2009 [65], a more advanced and most likely cheaper conductor was proposed. It is based on high purity aluminum alloys, such as Al-0.1%Ni, which were used in the ATLAS central solenoid. Figure 27 shows a cross sections of the CMS conductor and of an advanced SiD conductor design using Al-0.1%Ni and novel internal high strength stainless steel reinforcement. Other conductor stabilizer possibilities are also under consideration and study. These include TiB_2 grain refinement aluminum matrix composites, and cold work hardening via the equal area angle extrusion process

2023 JINST 18 T06013

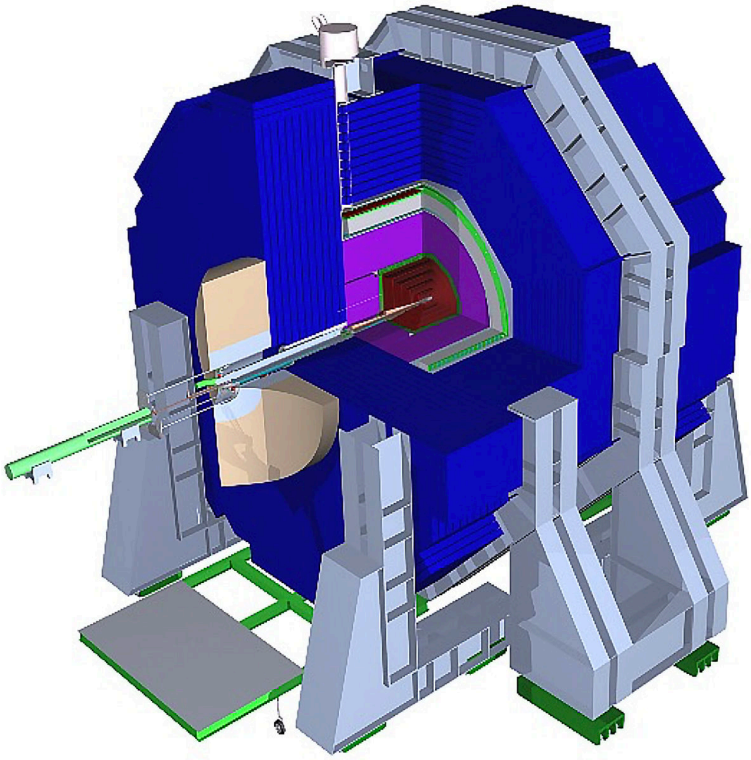

Figure 25. Overview of the SiD.

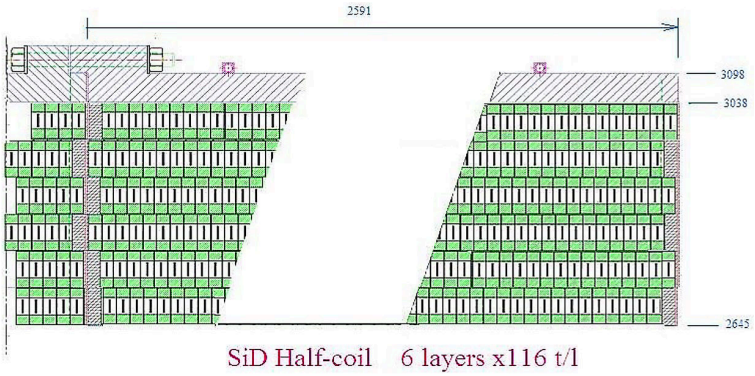

Figure 26. The SiD coil winding design. The cooling pipes are shown welded to the outer support cylinder; the two modules are joined by bolting at the median plane.

4.2 Detectors for secondary particle experiments

4.2.1 COMET

The COMET experiment in J-PARC aims to explore the rare decay phenomenon of muons. Figure 28 shows the overview of COMET Phase-I beam line. In order to transport the muons effectively, the superconducting solenoids are used throughout the muon beamline from the target to generate pion, to the electron detectors, that is, the Pion Capture Solenoid (PCS), Muon Transport Solenoid (MTS), Bridge Solenoid (BS) and Detector Solenoid (DS). A smooth variation of the magnetic field across

2023 JINST 18 T06013

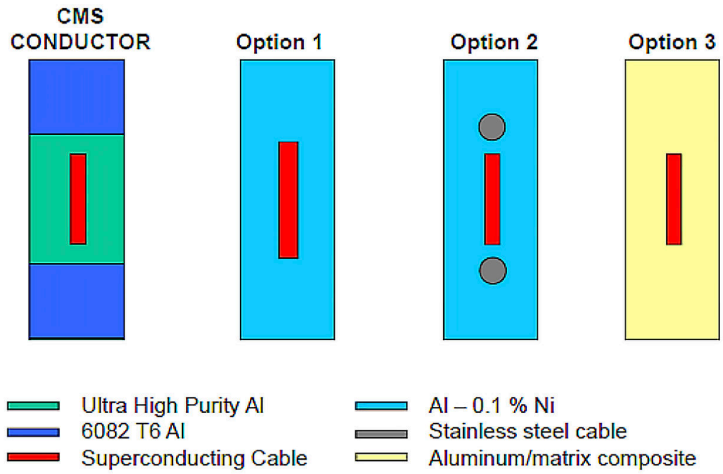

Figure 27. Cross sections of CMS conductor and proposed SiD conductors.

the beam line is required, in paticular at the transitions between magnets where muons may be trapped or reflected. Figure 29 shows the magnetic field distribution on the muon beam axis. The solenoids are aligned in such a way that the ripple of magnetic field would be less than 5 % of averaged field in each section. All the solenoids are covered by iron yokes, which are used as both radiation shield and magnetic flux return yoke. Figure 30 shows the 3D view of DS for COMET Phase-I experiment. The detector solenoid acts as a spectrometer of the electrons generated by the decay of muons, and all the electron detectors are installed inside the magnet bore. The detector solenoid is conventional solenoid wound by copper-stabilized Nb-Ti conductor cooled by GM cryocoolers. The total length of superconducting coil is 1.9 m, the inner bore diameter of coil is 2.14 m. The superconducting coil consists of 14 coils 170 mm in length and 8 mm in thickness. All the coils are connected in series, and the nominal current is 189 A to generate the central field of 1 T. The inductance of the detector solenoid is 236 H, which is too large to extract the stored energy into the dump resistor for the quench protection, therefore, the quench protection by a passive heater is adopted. Figure 31 shows the quench protection circuit of DS. Heater wire of 1.5 mm in diameter is wound on the outside of superconducting coils, and the heaters are connected in parallel with coils as shown in figure 31. When a quench is detected by the quench detection system, the power supply is cut off by the circuit breaker, and the magnet current go through the heaters. Thanks to the quick quench propagation by the heaters, the maximum temperature in the coil can be suppressed below 150 K during a quench.

The PCS is not a detector solenoid, but the technology of the detector magnet is adopted, such as, the superconducting cable stabilized with high purity aluminum [66]. The PCS contains the pion production target, and it is exposed to high radiation, meaning that large heat load is expected into the coils, calculated to be 228 W at maximum in the Phase-II experiment. In addition, conduction cooling scheme is applied in order to reduce the exposure of the liquid helium to direct radiation. The Nb-Ti with copper stabilizer based thick aluminum stabilized cable is used in the PCS; 15 mm in width, 4.7 mm in thickness and composition ratio of Al/Cu/Nb-Ti is 7.3/0.9/1.0. The magnets are cooled down by cooling pipes flowing two-phase liquid helium on the outer surface of the coil shell, and the pure aluminum strips are sandwiched between layers as shown in figure 32, to help the removal of radiation heat.

2023 JINST 18 T06013

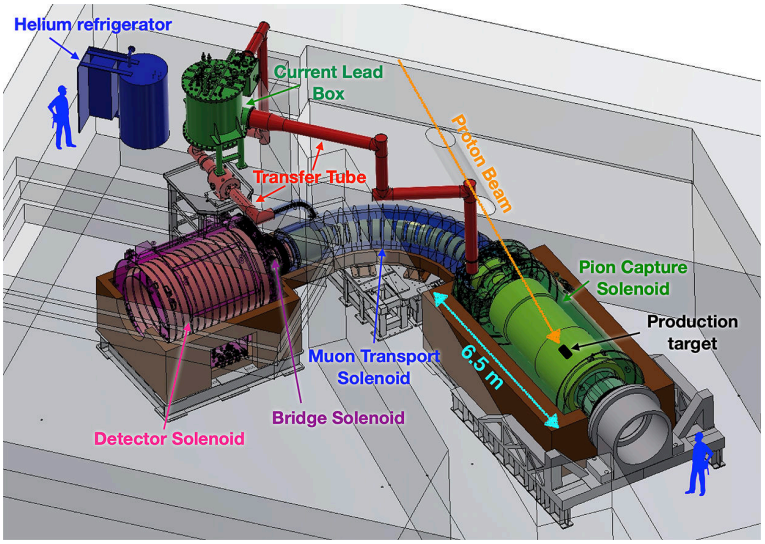

Figure 28. Overview of COMET beam line for Phase-I experiment.

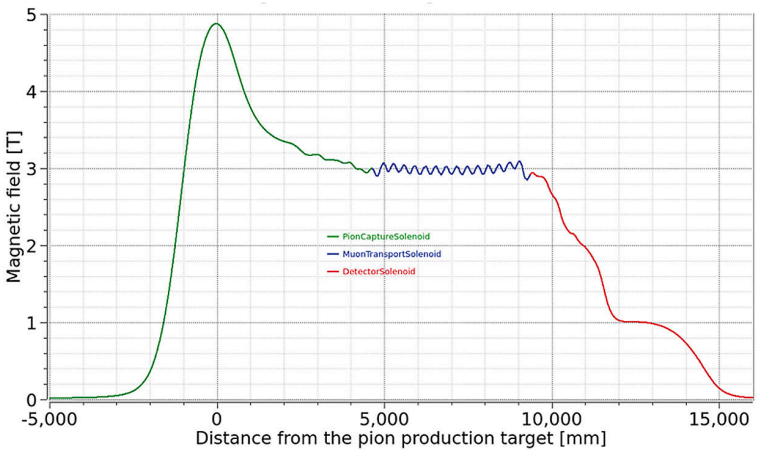

Figure 29. Magnetic field distribution of COMET beam line for Phase-I experiment.

4.2.2 J-PARC *g*-2/EDM

In the J-PARC *g*-2/EDM experiment, the detector solenoid is also used as muon storage magnet. Positive muons are stored in the magnet, and decay positrons of polarized $\mu+$ are measured. The decay positrons are detected by silicon strip detectors placed inside the muon storage orbit. One unique feature of the magnet is to adopt the three-dimensional spiral injection scheme. The muon beam enters the solenoid from the top end, and spirally go down to the storage region around the magnet center. When the beam crosses the storage region, magnetic field to kick the beam is applied to store the beam in the storage region. A very small static weak-focusing field is also applied around the storage region to maintain the beam in the storage region. Specifications required for magnetic field is summarized as follows;

- Storage regions

2023 JINST 18 T06013

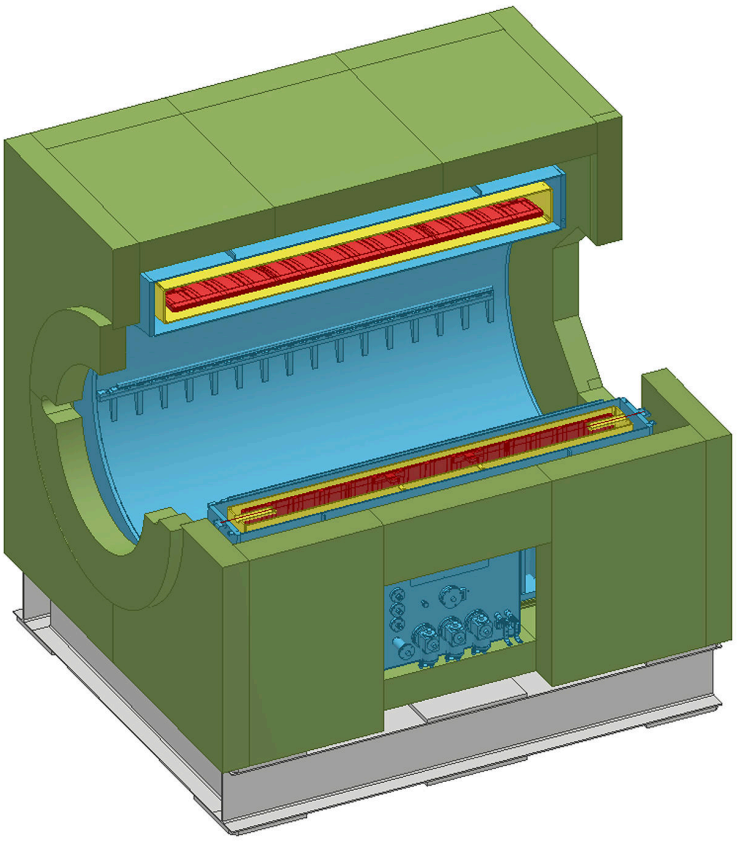

Figure 30. COMET DS magnet.

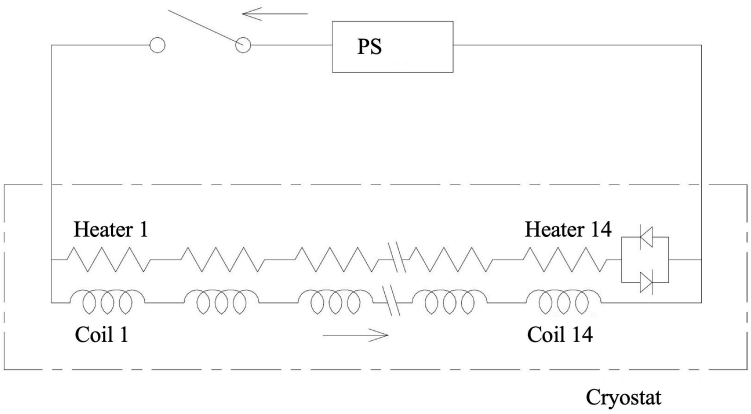

Figure 31. Quench protection circuit of COMET DS magnet.

  - Axial magnetic field: 3 T
  - Uniformity: < 1 ppm locally, < 0.1 ppm in circumferential average
  - Region: 33.3 ± 1.5 cm in radius, ± 5 cm in height

- Injection regions

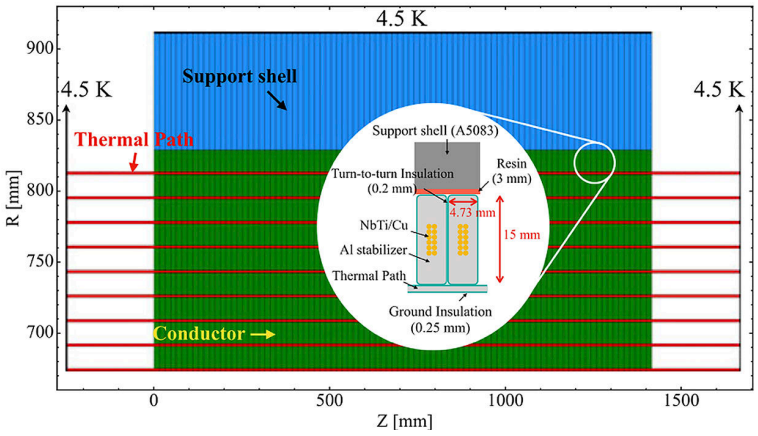

Figure 32. Cross sectional view of one PCS coil. Red, green, and blue regions indicate the aluminum strip, conductor and support shell, respectively.

- $B_r \times B_z > 0$
- Radial field has to change smoothly along the beam orbit
- Region: from the end of the beam injection line to the beam storage region

• Weak focus field

- In the storage region,

$$B_z = B_0 - n\frac{B_{0z}}{R}r + n\frac{B_{0z}}{2R_0^2}z^2, \tag{4.1}$$

- n: n-index $\sim (1.5 \pm 0.5) \times 10^{-4}$

The important feature of the superconducting magnet is the magnetic field homogeneity in the storage region, less than 1 ppm locally and 0.1 ppm in circumferential average. In order to satisfy the requirement, new analytical code using truncated singular value decomposition method to optimize coil position and size is being newly developed [68], and the design work is in progress using both the new code and existing commercial FEM code that can calculate with non-linear effect. The present design of the magnet system is shown in figure 33. The superconducting main, shim and weak focusing coils are wound with a Nb-Ti wire with copper stabilizer. Main characteristics of the magnet are summarized in table 8. A superconducting switch is also connected with the main coils and these are operated in persistent current mode so that the magnetic field fluctuation caused by a voltage ripple of power supply can be ignored. All superconducting coils are cooled by liquid helium in cryostat to keep coil temperature constant. GM cryocoolers are attached to the cryostat to minimize evaporation of liquid helium, and decrease the change of temperature distribution in the coils. Iron yoke covers the superconducting magnet to decrease the effect of ferromagnetic material outside the magnet on the field homogeneity, and iron yoke with cylindrical poles to make the homogeneous magnetic field in the storage region with ring shape.

The magnet is operated in persistent current mode as described above, and it means that the stored energy must be mainly dissipated during quench. In order to decrease the current decay time, and enhance the quench propagation by utilizing AC loss in superconductor, small loops

2023 JINST 18 T06013

are made using diodes as shown in figure 34. The loops are adjusted in such a way that the self and mutual inductance match each other. The simulated temperature and voltage in the coils are shown in figure 35. The peak temperature and voltage are calculated to be around 180 K and 1.6 kV, respectively, indicating that the magnet could be safely protected from the quench.

These 3-D magnetic field design and control technologies are being developed in collaboration with Ibaraki University. Accompanying the precise magnetic field control, precise magnetic field monitoring system development is necessary. US-JP collaboration on the NMR magnetometer with ultra-high precision [69] is in progress effectively.

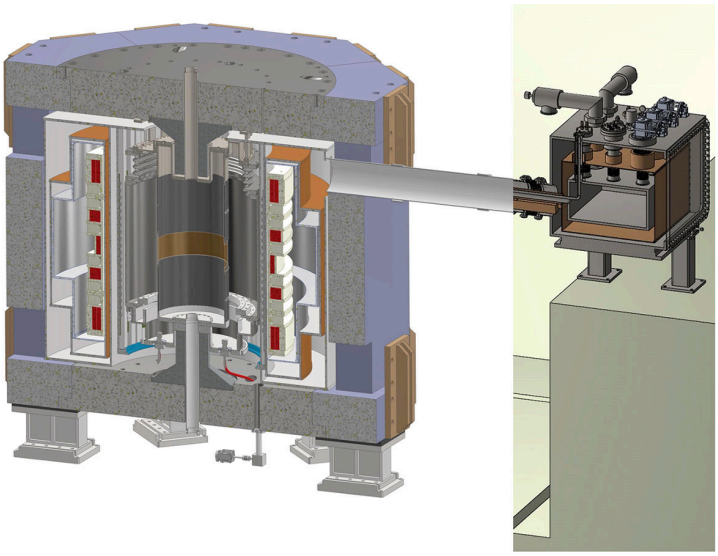

Figure 33. J-PARC g-2/EDM magnet overview.

Table 8. Main parameters of the storage magnet.

Item	Unit	Value
Nominal current	A	423.4
Stored energy	MJ	17.2
Magnet inductance	H	198
Peak field on SC coil	T	4.9

5 Summary

Various superconducting detector solenoids for particle physics were developed since the 1970's. A key technology is the aluminum stabilized superconducting cable for the almost all the detector magnets in particle physics experiments. With the progress of Al-stabilized conductor, the coil fabrication technology has been also advanced, that is, the inner winding technology directly inside the support cylinder, indirect cooling scheme, utilization of pure aluminum strips for the safe quench protection, and so on. The vacuum vessel design study were also developed, especially in transparent detector solenoids, e.g., isogrid type and honeycomb type vacuum vessels. These technologies

2023 JINST 18 T06013

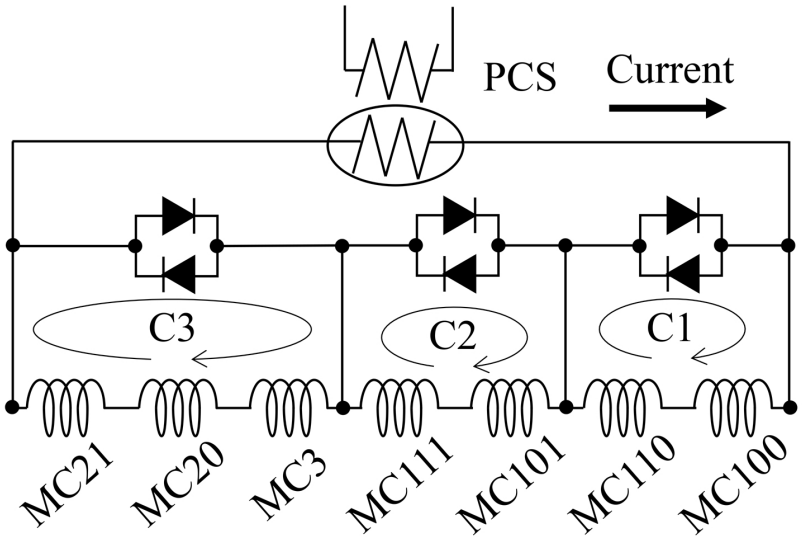

Figure 34. Electrical circuit for the J-PARC g-2/EDM magnet.

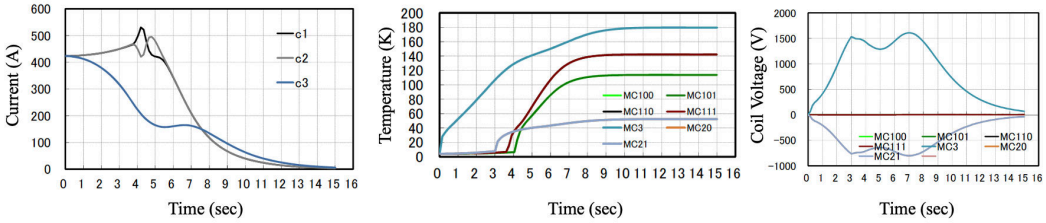

Figure 35. Quench simulation results.

were used successfully for the manufacturing of many superconducting detector magnets in the past four decades thanks to the technical and scientific competencies developed, with many regular breakthroughs. The detector solenoids design study is in progress for future big projects in Japan and Europe, that is, ILC, FCC and CLIC, based on the technologies developed over many years. The magnet size for each project is as large as or larger than the magnets, like CMS and ATLAS-CS, and higher strength while keeping higher RRR is a key point for the development of Al-stabilized conductor. In addition, the larger current capacity is required accompanying with the larger bore size. The ILC and FCC groups are continuing the design study of the conductor. The present concern for the detector solenoid development is to nearly lose the key technologies and experience. Complementary efforts are needed to reach again an equivalent level of expertise, to continue the effort on research and to develop these technologies and apply them to each future detector magnet project, especially, for the development of Al-stabilized conductor fabrication. A worldwide collaboration is needed to reach and validate the required performances. KEK and CERN jointly held a workshop to share the awareness of industrial issue of the Al-stabilized conductor fabrication, in which, all stakeholders were invited, including superconducting magnet scientists, engineers of conductor industries and physicists who plan and design the future particle experiments. At

2023 JINST 18 T06013

the workshop, the current situation of Al-stabilized conductor availability was shared, and the future possibility to resume the manufacture of Al-stabilized conductor was discussed. Workshop participants agreed to continue the world-wide effort to explore the availability of the conductor. For the detector solenoids for mid-scale experiments using a conventional copper-stabilized Nb-Ti conductor, specific features like precise control of magnetic field distribution, might be required. The development efforts are on-going in terms of the magnetic field design technology with high precision simulation, the coil fabrication technology to achieve the design requirement and the control method of magnetic field distribution.

References

[1] A. Yamamoto and Y. Makida, *Advances in superconducting magnets for high energy and astroparticle physics*, *Nucl. Instrum. Meth. A* **494** (2002) 255.

[2] M. Morpurgo, *Design and Construction of a Pump for Liquid Helium*, *Cryogenics* **17** (1977) 91.

[3] H. Desportes, J. Le Bars and G. Mayaux, *Construction and Test of the 'Cello' Thin Wall Solenoid*, *Adv. Cryog. Eng.* **25** (1980) 175.

[4] M.A. Green, *The role of quench back in quench protection of a superconducting solenoid*, *Cryogenics* **24** (1984) 659.

[5] CDF collaboration, *Construction and testing of a 3-m diameter × 5-M superconducting solenoid for the Fermilab collider detector facility (CDF)*, *Nucl. Instrum. Meth. A* **238** (1985) 18.

[6] A. Yamamoto et al., *Performance of the TOPAZ Thin Superconducting Solenoid Wound with Internal Winding Method*, Tech. Rep. KEK-PREPRINT-85-83 (1986) [*Jpn. J. Appl. Phys.* **25** (1986) 440].

[7] R. Arai, O. Araoka, Y. Doi, T. Haruyama, N. Ishihara, M. Kawai et al., *Test operations of the VENUS superconducting magnet at KEK*, *Nucl. Instrum. Meth. A* **254** (1987) 317.

[8] J.M. Baze et al., *Design, construction and test of the large superconducting solenoid ALEPH*, *IEEE Trans. Magn.* **24** (1988) 1260.

[9] P.T.M. Clee and D.E. Baynham, *Towards the realization of two 1.2 tesla superconducting solenoids for particle physics experiments*, in *Proceedings of the 11th International Conference on Magnet Technology*, Tsukuba, Japan, 28 August–1 September 1989, pp. 206–211.

[10] A. Bonito Oliva, O. Dormicchi, M. Losasso and Q. Lin, *ZEUS thin solenoid: Test results analysis*, *IEEE Trans. Magn.* **27** (1991) 1954.

[11] C.M. Monroe, J.S.H. Ross, G.E. Shrimpton and K.D. Smith, *The CLEO II Magnet — Design, Manufacture and Tests*, in *Proceedings of the Twelfth International Cryogenic Engineering Conference*, Southampton, U.K., 12–15 July 1988, pp. 773–779.

[12] A. Yamamoto et al., *Development of a prototype thin superconducting solenoid magnet for the SDC detector*, *IEEE Trans. Appl. Supercond.* **5** (1995) 849.

[13] L.M. Barkov, N.S. Bashtovoy, S.V. Karpov, V.S. Okhapkin, A.A. Ruban, V.P. Smakhtin et al., *Superconducting rectifier fluxpump for magnet system of the CMD-2 detector*, *IEEE Trans. Appl. Supercond.* **9** (1999) 4585.

[14] A. Yamamoto et al., *Progress in ATLAS central solenoid magnet*, *IEEE Trans. Appl. Supercond.* **10** (2000) 353.

2023 JINST 18 T06013

[15] A. Hervé et al., *Status of the construction of the CMS magnet*, *IEEE Trans. Appl. Supercond.* **14** (2004) 542.

[16] Y. Makida et al., *The BESS-Polar Ultra-Thin Superconducting Solenoid Magnet and Its Operational Characteristics During Long-Duration Scientific Ballooning Over Antarctica*, *IEEE Trans. Appl. Supercond.* **19** (2009) 5067034.

[17] A. Yamamoto, Y. Makida, K.-i. Tanaka, Y. Doi, T. Kondo, K. Wada et al., *Development towards ultrathin superconducting solenoid magnets for high-energy particle detectors*, *Nucl. Phys. B Proc. Suppl.* **78** (1999) 565.

[18] K. Wada, S. Meguro, H. Sakamoto, T. Shimada, Y. Nagasu, I. Inoue et al., *Development of high-strength and high-RRR aluminum-stabilized superconductor for the ATLAS thin solenoid*, *IEEE Trans. Appl. Supercond.* **10** (2000) 373.

[19] A. Yamamoto and T. Taylor, *Superconducting Magnets for Particle Detectors and Fusion Devices*, in *Reviews of Accelerator Science and Technology - Volume 5: Applications of Superconducting Technology to Accelerators*. World Scientific Publishing Co. Pte. Ltd (2012), pp. 91–118.

[20] M. Wilson, *Superconducting Magnet*, Oxford Science Publishing (1987), IBBN: 0-19-85-4810-K.

[21] A. Yamamoto et al., *Development of a prototype thin superconducting solenoid magnet for the SDC detector*, *IEEE Trans. Appl. Supercond.* **5** (1995) 849.

[22] H. Yamaoka, A. Yamamoto, Y. Makida, K. Tanaka, T. Kondo, I. Ohno et al., *Development of a brazed aluminum honeycomb vacuum vessel for a thin superconducting solenoid magnet*, *Adv. Cryog. Eng.* **39** (1994) 1983.

[23] R.W. Fast, C.P. Grozis, A. Lee and R.H. Wands, *Isogrid vacuum shell for large superconducting solenoid*, *Adv. Cryog. Eng.* **39** (1994) 1991.

[24] Particle Data Group collaboration, *Review of Particle Physics*, *Prog. Theor. Exp. Phys.* **2022** (2022) 083C01.

[25] M. Gupta, *Calculation of radiation length in materials*, Tech. Rep. CERN-PH-EP-Technical-Note-2010-013, CERN, Genva, Switzerland (2010).

[26] N. Cure et al., private communication.

[27] M. Gonzalez et al., *Low mass cryostat for HEP experiments*, *CERN EP R&D report* (2021), https://indico.cern.ch/event/1063927/contributions/4560075/subcontributions/354326/attachments/2343874/3996348/20211111_WP4_Cryostat.pdf.

[28] S. Sgobba, D. Campi, B. Curé, P. El-Kallassi, P. Riboni and A. Yamamoto, *Toward an Improved High Strength, High RRR CMS Conductor*, *IEEE Trans. Appl. Supercond.* **16** (2006) 521.

[29] G. Aglieri et al., *Strategic R&D Programme on Technologies for Future Experiments - Annual Report 2020*, Tech. Rep. CERN-EP-RDET-2021-001 10.17181/CERN-EP-RDET-2021-001.

[30] T. Ogitsu, T. Nakamoto, K.-i. Sasaki, M. Sugano, M. Iio, K. Suzuki et al., *R&D works for Superconducting Magnet for Future Accelerator Applications in Japan*, in *Proceedings of SNOWMASS 2021* arXiv:2203.12118.

[31] M. Benedikt et al., *Future Circular Colliders*, *Ann. Rev. Nucl. Part. Sci.* **69** (2019) 389.

[32] *LHC Design Report Vol.1: The LHC Main Ring*, Tech. Rep. CERN-2004-003-V1 (2004), 10.5170/CERN-2004-003-V-1.

[33] G.F. Giudice, ed., *Fifty years of research at CERN: From past to future*, *CERN Yellow Reports: Monographs*, Tech. Rep. CERN-2006-004, CERN, Geneva, Switzerland (2006).

2023 JINST 18 T06013

[34] A. Abada, M. Abbrescia, S.S. AbdusSalam, I. Abdyukhanov, J. Abelleira Fernandez, A. Abramov et al., *FCC-ee: The Lepton Collider. Future Circular Collider Conceptual Design Report Volume 2*, *Eur. Phys. J. ST* **228** (2019) 261.

[35] RD-FA collaboration, *IDEA: A detector concept for future leptonic colliders*, *Nuovo Cim. C* **43** (2020) 27.

[36] N. Alipour Tehrani et al., *CLICdet: The post-CDR CLIC detector model*, Tech. Rep. CLICdp-Note-2017-001, CERN, Geneva, Switzerland (2017), revised 2019.

[37] A. Yamamoto et al., *The ATLAS central solenoid*, *Nucl. Instrum. Meth. A* **584** (2008) 53.

[38] A. Herve, *Construction a 4-Tesla large thin solenoid at the limit of what can be safely operated*, *Mod. Phys. Lett. A* **25** (2010) 1647.

[39] N. Deelen, A. Dudarev, B. Curé and M. Mentink, *Design and Quench Analysis of Superconducting Solenoids for the Lepton Future Circular Collider*, *IEEE Trans. Appl. Supercond.* **32** (2022) 4100204.

[40] A. Yamamoto et al., *A thin superconducting solenoid magnet for particle astrophysics*, *IEEE Trans. Appl. Supercond.* **12** (2002) 438.

[41] S. Sgobba, C. D'Urzo, P. Fabbricatore and S. Sequeira Tavares, *Mechanical performance at cryogenic temperature of the modules of the external cylinder of CMS and quality controls applied during their fabrication*, *IEEE Trans. Appl. Supercond.* **14** (2004) 556.

[42] A. Perin, R. Macias Jareno and L. Metral, *Study of materials and adhesives for superconducting cable feedthroughs*, *AIP Conf. Proc.* **613** (2002) 551.

[43] FCC collaboration, *FCC-hh: The Hadron Collider: Future Circular Collider Conceptual Design Report Volume 3*, *Eur. Phys. J. ST* **228** (2019) 755.

[44] M. Mentink, H. Silva, A. Dudarev, E. Bielert, V. Klyukhin, B. Cure et al., *Evolution of the Conceptual FCC-hh Baseline Detector Magnet Design*, *IEEE Trans. Appl. Supercond.* **28** (2018) 2782708.

[45] CLICdp, CLIC collaboration, *The Compact Linear Collider (CLIC) - 2018 Summary Report*, Tech. Rep. CERN-2018-005-M (12, 2018), 10.23731/CYRM-2018-002.

[46] A. Robson, P.N. Burrows, N. Catalan Lasheras, L. Linssen, M. Petric, D. Schulte et al., *The Compact Linear e^+e^- Collider (CLIC): Accelerator and Detector*, arXiv:1812.07987.

[47] V. Cilento, R. Tomás, B. Cure, A. Faus-Golfe, B. Dalena and Y. Levinsen, *Dual beam delivery system serving two interaction regions for the Compact Linear Collider*, *Phys. Rev. Accel. Beams* **24** (2021) 071001.

[48] CMS collaboration, *CMS, the magnet project: Technical design report*, Tech. Rep. CERN-LHCC-97-10, CERN, Geneva, Switzerland (1997).

[49] ATLAS collaboration, *ATLAS central solenoid: Technical design report*, Tech. Rep. CERN-LHCC-97-21, CERN, Geneva, Switzerland (1997).

[50] B. Curé, B. Blau, A. Hervé, P. Riboni, S.S. Tavares and S. Sgobba, *Mechanical properties of the CMS conductor*, *IEEE Trans. Appl. Supercond.* **14** (2004) 530.

[51] S.A.E. Langeslag, B. Curé, S. Sgobba, A. Dudarev, H.H.J. ten Kate, J. Neuenschwander et al., *Effect of thermo-mechanical processing on the material properties at low temperature of a large size Al-Ni stabilized Nb-Ti/Cu superconducting cable*, *AIP Conf. Proc.* **1574** (2014) 211.

[52] K. Wada, S. Meguro, H. Sakamoto, A. Yamamoto and Y. Makida, *High-strength and high-RRR Al-Ni alloy for aluminum-stabilized superconductor*, *IEEE Trans. Appl. Supercond.* **10** (2000) 1012.

2023 JINST 18 T06013

[53] B. Cure and I. Horvath, *Developments of electrical joints for aluminum-stabilized superconducting cables*, *IEEE Trans. Appl. Supercond.* **9** (1999) 197.

[54] S. Farinon, P. Chesny, B. Cure, P. Fabbricatore, M. Greco and R. Musenich, *Electrical joints in the CMS superconducting magnet*, *IEEE Trans. Appl. Supercond.* **12** (2002) 462.

[55] L. Linssen, A. Miyamoto, M. Stanitzki and H. Weerts, eds., *Physics and Detectors at CLIC: CLIC Conceptual Design Report*, Tech. Rep. CERN-2012-003 (2012), 10.5170/CERN-2012-003.

[56] A. Ballarino, *HTS current leads: Performance overview in different operating modes*, *IEEE Trans. Appl. Supercond.* **17** (2007) 2282.

[57] X. Chen, J. Jin, J. Liu, H. Ren and T. Xiang, *Development and techniques of high current leads for HTS device applications*, in *Proceedings of International Conference on Applied Superconductivity and Electromagnetic Devices*,Chengdu, China , 25–27 September 2009, pp. 34–41.

[58] A. Ballarino, *Development of superconducting links for the Large Hadron Collider machine*, *Supercond. Sci. Technol.* **27** (2014) 044024.

[59] M. Bonura, C. Barth and C. Senatore, *Electrical and Thermo-Physical Properties of Ni-Alloy Reinforced Bi-2223 Conductors*, *IEEE Trans. Appl. Supercond.* **29** (2019) 1.

[60] ILD collaboration, *The ILD detector at the ILC* [arXiv:1912.04601].

[61] ILD collaboration, The ILD concept grpup, *The ILD detector at the ILC*, https://www.snowmass21.org/docs/files/summaries/EF/SNOWMASS21-EF0_EF0-IF0_IF0_Ties_Behnke_(ILD_group)-145.pdf

[62] F. Kircher et al., *Conceptual design of the ILD detector magnet system*, Tech. Rep. LC-DET-2018-081, DESY, Hamburg, Germany (2018)

[63] M. Breidenbach, J.E. Brau, P. Burrows, T. Markiewicz, M. Stanitzki, J. Strube et al., *Updating the SiD Detector concept*, arXiv:2110.09965.

[64] R.P. Smith and R.H. Wands, *A Five Tesla Solenoid With Detector Integrated Dipole for the Silicon Detector at the International Linear Collider*, *IEEE Trans. Appl. Supercond.* **16** (2006) 489.

[65] H. Aihara, P. Burrows and M. Oreglia, eds., *SiD Letter of Intent*, Tech. Rep. SLAC-R-989, FERMILAB-LOI-2009-01, FERMILAB-PUB-09-681-E [arXiv:0911.0006].

[66] M. Yoshida et al., *Status of Superconducting Solenoid System for COMET Phase-I Experiment at J-PARC*, *IEEE Trans. Appl. Supercond.* **25** (2015) 4500904.

[67] Y. Yang, M. Yoshida, M. Iio, K.-i. Sasaki, T. Ogitsu, T. Nakamoto et al., *Study of Irradiation Effects on Thermal Characteristics for COMET Pion Capture Solenoid*, *IEEE Trans. Appl. Supercond.* **28** (2018) 4001405.

[68] M. Abe and K. Shibata, *Coil Block Designs With Good Homogeneity for MRI Magnets Based on SVD Eigenmode Strengths*, *IEEE Trans. Magn.* **51** (2015) 2412515.

[69] H. Yamaguchi et al., *Development of a CW-NMR Probe for Precise Measurement of Absolute Magnetic Field*, *IEEE Trans. Appl. Supercond.* **29** (2019) 9000904.

2023 JINST 18 T06013